SPi	Journal Code				Article ID				Dispatch: 26.01.13	CE: Area not defined
	G	B	C		2	0	0	0	No. of Pages: 13	ME:

GLOBAL BIOGEOCHEMICAL CYCLES, VOL. 27, 1–13, doi:10.1002/gbc.20004, 2013

Basin scale survey of marine humic fluorescence in the Atlantic: relationship to iron solubility and H_2O_2

M. I. Heller,[1,4] D. M. Gaiero,[2] and P. L. Croot[1,3]

Received 11 June 2012; revised 16 October 2012; accepted 12 November 2012.

[1] Iron (Fe) is a limiting nutrient for phytoplankton productivity in many different oceanic regions. A critical aspect underlying iron limitation is its low solubility in seawater as this controls the distribution and transport of iron through the ocean. Processes which enhance the solubility of iron in seawater, either through redox reactions or organic complexation, are central to understanding the biogeochemical cycling of iron. In this work we combined iron solubility measurements with parallel factor (PARAFAC) data analysis of Coloured Dissolved Organic Matter (CDOM) fluorescence along a meridional transect through the Atlantic (PS ANT XXVI-4) to examine the hypothesis that marine humic fluorescence is a potential proxy for iron solubility in the surface ocean. PARAFAC analysis revealed 4 components (C1-4), two humic like substances (C2&4) and two protein-like (C1&3). Overall none of the 4 components were significantly correlated with iron solubility, though humic-like components were weakly correlated with iron solubility in iron replete waters. Our analysis suggests that the ligands responsible for maintaining iron in solution in the euphotic zone are sourced from both remineralisation processes and specific ligands produced in response to iron stress and are not easily related to bulk CDOM properties. The humic fluorescence signal was sharply attenuated in surface waters presumably most likely due to photo bleaching, though there was only a weak correlation with the transient photo product H_2O_2, suggesting longer lifetimes in the photic zone for the fluorescent components identified here.

Citation: Heller, M. I., D. M. Gaiero, and P. L. Croot (2013), Basin scale survey of marine humic fluorescence in the Atlantic: relationship to iron solubility and H_2O_2, *Global Biogeochem. Cycles*, *27*, doi:10.1002/gbc.20004.

1. Introduction

[2] The solubility of iron in seawater is a major control on the formation of colloidal and particulate iron and in turn on the bioavailability of iron to phytoplankton. Inorganic iron is poorly soluble in oxygenated seawater [*Kuma et al*., 1996; *Liu and Millero*, 2002] and is observed to be as low as 20 pmol L^{-1} at pH 8.1, 25°C. Thus Fe(III), the thermodynamic favored form of Fe under oxygenated conditions in seawater is rapidly scavenged and forms various Fe(III)-oxyhydroxides. However in the presence of strong organic Fe binding ligands the solubility is raised to nM levels [*Kuma et al*., 1996; *Liu and Millero*, 2002]. Fe(II) is the more bioavailable fraction of iron [*Shaked et al*., 2005] but is mostly present as a reactive intermediate in Fe cycling under ambient seawater conditions due to its rapid oxidation by O_2 and H_2O_2 [*Santana-Casiano et al*., 2006]. Presently however there is very little information on the key processes, and the rates, by which Fe is converted to, or maintained in, soluble forms. Similarly there is a lack of data on the sources and sinks for the organic ligands that complex Fe in seawater.

[3] A promising area of research is the apparent correlation found previously in intermediate and deep waters of the Pacific between Fe solubility, nutrient concentrations, apparent oxygen utilization (AOU) and humic fluorescence (HFlu) [*Hayase and Shinozuka*, 1995; *Kuma et al*., 1998]. This relationship has been interpreted as indicating release of organic metal chelators from the remineralization of particulate matter. Thus these organic chelators are a fraction of the dissolved organic matter (DOM) in the ocean. DOM is a complex mix of organic molecules and is poorly described in terms of it composition. Chromophoric Dissolved Organic Matter (CDOM) is the proportion of DOM that absorbs light and this is easily characterized by its absorbance and fluorescence properties [*Coble*, 2007]. The CDOM fluorescence signals observed in seawater can generally be divided into two categories [*Coble*, 1996]; humic-type or protein/amino acid-type fluorescence. Multiple components can be determined using Excitation Emission Matrix (EEM) fluorescence methods combined with parallel factor (PARAFAC) data analysis [*Stedmon and Bro*, 2008]. Humic-like fluorescence

[1]Helmholtz Centre for Ocean Research Kiel (GEOMAR), FB2 Marine Biogeochemistry, Chemical Oceanography, Kiel, Germany.
[2]CICTERRA/Universidad Nacional de Còrdoba, Chemistry Department, Còrdoba, Argentina.
[3]Earth and Ocean Sciences, School of Natural Sciences, National University of Ireland Galway (NUI-Galway), Galway, Ireland.
[4]Now at University of Southern California, Los Angeles, California, USA.

Corresponding author: M. I. Heller, Helmholtz Centre for Ocean Research Kiel (GEOMAR), FB2 Marine Biogeochemistry, Chemical Oceanography, Kiel, Germany. (miheller@usc.edu)

0886-6236/13/10.1002/gbc.20004

has been observed in a wide range of marine environments, and in general correlates well with nutrients (NO_3^-, PO_4^{3-}) and apparent oxygen utilization (AOU) in different water masses [*Hayase and Shinozuka*, 1995; *Kuma et al*., 1998; *Yamashita and Tanoue*, 2008; *Yamashita et al*., 2007]. These correlations suggest that the components that make up fluorescent CDOM are formed by the remineralization of settling organic particles and are destroyed or modified by irradiation.

[4] Marine humic substances are composed of a large fraction of the uncharacterized DOM in the ocean [*Zafiriou et al*., 1984] but the relative contribution of these complex substances to seawater fluorescence is still unclear. The complexation of iron by terrestrial humic acids has been shown to increase iron solubility at pH 8 in NaCl solutions [*Liu and Millero*, 1999]. Recent research suggests that due to the tight correlation between humic-type fluorescence and iron solubility in vertical profiles, that substances with humic character could have a strong iron-binding capacity and thus be a control on Fe(III) solubility and dissolved iron concentrations in seawater [*Kitayama et al*., 2009; *Nakayama et al*., 2011; *Nishimura et al*., 2012; *Takata et al*., 2004; *Tani et al*., 2003]. In the present work we investigate the links between Fe solubility and fluorescence based estimates of marine humic levels using both a single wavelength approach [*Tani et al*., 2003] and using multiple wavelengths by PARAFAC [*Jørgensen et al*., 2011].

[5] Links between bulk DOM and iron solubility have also been reported; *Chen et al.* [2004] reported data showing a linear relationship between dissolved organic carbon (DOC) concentrations and iron solubility. More recently *Wagener et al.* [2008] suggested that DOC had an impact on the dissolution of dust in surface waters at a time series site in the Mediterranean. They found that the dissolution rate of iron from atmospheric dust was linearly dependent on iron binding ligands and DOC concentrations. Similar work [*Heller and Croot*, 2011] close to Cape Verde in the Tropical Eastern Atlantic has shown similar temporal variations in iron speciation and reactivity during dust deposition experiments. These later studies suggest that the iron binding and therefore solubility may be highly variable in surface waters.

[6] CDOM absorption of sunlight in the euphotic zone leads to excited triplet states which can react with triplet O_2 to form O_2^- and carbocations [*Heller and Croot*, 2010a; *O'Sullivan et al*., 2005]. Photo-produced O_2^- is the dominant source of H_2O_2 in the euphotic zone through reactions with trace metals and CDOM [*Heller and Croot*, 2010b; 2010c]. At present there is little information regarding links between CDOM fluorescence and the formation of H_2O_2 in the ocean. It is well known that photo-oxidation of Tryptophan produces O_2^- and subsequently H_2O_2 [*McCormick and Thomason*, 1978], reactions with other photo-produced reactive oxygen species (ROS) (e.g. $^1O_2$ and OH) may also be important pathways for the destruction of proteins, and hence the loss of protein-like fluorescence, in the ocean [*Boreen et al*., 2008]. Similarly the loss of HFlu in surface waters is often ascribed to photo-bleaching [*Omori et al*., 2011] but only a few studies have examined the production of H_2O_2 from marine humics [*Amador et al*., 1990; *Cooper et al*., 1988].

[7] The present work seeks to examine the relationship between the distribution and properties of fluorescence substances, including humics, and iron solubility under ambient conditions in the epipelagic and upper part of the mesopelagic zone during an Atlantic Meridional Transect (AMT) which passed through regions which are impacted by different aeolian dust sources (e.g. Sahara and Patagonia). This study was performed in the context of a Deutsche Forschungsgemeinschaft (DFG) project, ADIOS-BAO (Atmospheric Dust and Irradiation effects on Ocean surface processes–Biogeochemistry in the Atlantic Ocean), in which the goal was to examine the influence of atmospheric dust deposition and irradiation on biogeochemical processes in the upper Atlantic ocean. The sampling program also included an occupation of the TENATSO ocean site (Tropical Eastern North Atlantic Time-Series Observatory, 17.59°N, 24.25°E; 3600 m water depth.) where we have performed related work [*Heller and Croot*, 2011] and a routine sampling program is maintained. The related TENATSO atmospheric observatory is located nearby on the island of Sao Vicente, Cape Verde.

2. Atlantic Meridional Transect–Dust Impacts on Biology

[8] A key area of research at present is focused on how iron and other biogeochemically important trace elements enter the ocean through atmospheric deposition [*Baker and Croot*, 2010; *Jickells et al*., 2005]. In this respect the Atlantic ocean is subject to an extremely wide range of deposition fluxes with low fluxes in the high latitude regions contrasting sharply with the highest fluxes found in the global ocean coincident with the passage of the Saharan Air Layer (SAL) over the Northern Tropical Atlantic [*Karyampudi et al*., 1999]. Iron supply has been hypothesized to limit N_2 fixation and hence oceanic primary productivity on geological timescales providing an alternative to phosphorus as the ultimate limiting nutrient [*Falkowski*, 1997]. Bioassay experiments in the eastern tropical North Atlantic showed that community primary productivity was N-limited, and that N_2 fixation was co-limited by iron and phosphorus [*Mills et al*., 2004]. The low aerosol flux to the equatorial South Atlantic leads to both lower rates of N_2 fixation [*Moore et al*., 2009] and lower abundances of the N_2-fixing, colonial cyanobacterium *Trichodesmium* [*Tyrrell et al*., 2003] in the South Atlantic than in the iron rich North Atlantic. Patagonian dust may also be an important source of Fe to the South Atlantic and Atlantic sector of the Southern Ocean [*Evangelista et al*., 2010; *Johnson et al*., 2011]. However along the continental shelf of South America, iron is supplied in roughly equivalent amounts from the atmosphere and coastal erosion, with a minor riverine component [*Gaiero et al*., 2007; *Gaiero et al*., 2003].

[9] The meridional distribution of CDOM absorbance in the major oceans was recently investigated by *Nelson et al.* [2010]. These authors found a positive correlation ($R^2 > 0.8$) between CDOM and AOU in the top 1000 m of the Pacific and Indian Ocean but a much weaker correlation for the Atlantic ($R^2 > 0.05$). A significant linear relationship (95%) was found between CDOM and other indices of organic matter remineralization (NO_3^-, PO_4^{3-}, TCO_2). However the transformation of dissolved materials cannot be the dominant source of CDOM, as <10% of AOU in deep waters result from DOC remineralization [*Aristegui et al*., 2002]. Differences in the CDOM distribution in the Pacific and Indian Oceans to the Atlantic Ocean have been explained by a combination of factors relating to circulation

and production. The surface water CDOM distribution of the North Atlantic is influenced by high CDOM waters (sub-arctic gyre, Arctic Ocean) and low CDOM waters (subtropical gyre) which are mixed in the water column by the formation of North Atlantic Deep Water [*Nelson et al*., 2007]. The rapid mixing in the Atlantic was found to dilute CDOM in its interior and this implies that the time scale for CDOM accumulation is greater than ~50 years. These ventilation rates exceed the rates of production which masks subsequently the correlation between CDOM and AOU. The apparent north-south symmetry of the Atlantic found along the A16 and A20 lines by *Nelson et al.* [2010] suggested to those authors that mixing processes, predominantly through the formation and transport of Antarctic Intermediate water, controlled the distribution of CDOM in the surface and intermediate waters of the South Atlantic.

3. Methodology

3.1. Sampling in the Water Column

[10] Samples were collected during the ANTXXVI-4 from 7 April to 17 May 2010 on board the German research vessel *R. V. Polarstern* on an AMT between Punta Arenas, Chile and Bremerhaven, Germany (Figure 1). Two short port calls were made in Mindelo, Cape Verde and Las Palmas, Canary Islands to exchange equipment and personnel. During the passage along the AMT a sampling station was occupied daily at local noon with a hydrocast down to 400 m. Samples were obtained throughout the upper 400 m for CDOM absorbance and fluorescence, HFlu, and H_2O_2 using standard Niskin bottles fitted to a seabird Conductivity-Temperature-Depth (CTD) rosette system. This system consisted of a SBE911plus CTD system in combination with a carousel water sampler SBE32 with 24 12-L bottles. In addition to this a transmissometer from Wetlabs and a Dr. Haardt Fluorometer (chlorophyll *a* fluorescence, denoted here as AFL, Figure 2) were used. The CTD system was equipped with a CT sensor pair. Unfortunately no O_2 sensor was installed on the CTD during this expedition.

[11] At 6 of the daily stations occupied during ANTXXVI-4 additional sampling was also performed for iron solubility (Figure 1). This involved trace metal clean sampling of seawater using modified Teflon coated PVC General Oceanics (Miami, FL, USA) GO-FLO bottles of 8 L deployed from the trace metal clean winch on the P.S. Polarstern. Immediately upon recovery of the bottles, samples were filtered in-line through 0.2 μm filter cartridges (Sartorious Sartobran filter capsule 5231307H5) by N_2 overpressure into acid cleaned 1 L Teflon bottles (Nalgene). Samples for CDOM and HFlu measurements were also obtained from these casts. All sampling and analysis was performed in a Class 5 sea going clean container (Clean Modules, UK).

3.2. Reagents and Labware

[12] Ultrapure (UP) water (R >18MΩ cm^{-1}) was obtained in the laboratory and in the sea going clean container via a Millipore Synergy 185 system that was fed by an Elix-3 (Millipore) reverse osmosis system connected to the mains supply. All equipment used for analysis were carefully cleaned with quartz distilled HCl (Q-HCl) and rinsed with UP before further use.

3.3. Iron Solubility Measurements

[13] The radioisotope ^{55}Fe is a weak beta emitter with a half-life of 2.7 years. The required radioisotope was received from Hartmann Analytics (Braunschweig, Germany). In this work the ^{55}Fe (Perkin Elmer) had a specific activity of 1985.42 mBq/mg Fe, a total activity of 75 mBq and a concentration of 1466.79 mBq/mL. The received ^{55}Fe isotope was dissolved in 0.1 m HCl and dilution standards were produced with UP water and acidified with Q-HCl to a pH < 2.

[14] The experimental protocol was principally the same as described previously [*Schlosser and Croot*, 2009], however the 0.02 μm Anotop syringe filter (Whatman) used previously was not available and so we were replaced them with Millipore MF 0.025 μm filters identical to those used in earlier solubility studies [*Kuma et al*., 1996; *Nakabayashi et al*., 2002]. The change in filter material required a new filtration system to be constructed. All the equipment used were Teflon and commercially available from Savillex. The filtration vessel was a 500 mL standard jar with transfer closure and two tube ports. On one of the tube ports a 47 mm filter holder and sample reservoir (200 mL) was connected with the appropriate adapters. To the second tube port of the jar, a trace metal clean vacuum pump (ILMVAC MPR060E) was connected, to achieve the required overpressure to pass the samples through the 0.025 μm filters. Duplicate samples of both filtered (0.025 μm) and unfiltered seawater (400 μL) were acidified and transferred into 6 mL vials in which 4.5 mL of scintillation fluid (Lumagel Plus®) were added. Sample storage, treatment and measurement were performed at room temperature (23°C) in the isotopic container located on the *RV Polarstern*. Iron solubility experiments were initiated within 3 hours of sample collection and run for upto 48 hours. Only the results after 48 hours are presented here. The activity of the ^{55}Fe solutions were determined by scintillation counting (Packard, Tri-Carb 2900TR) and then converted to soluble Fe concentrations, taking into account the activity of the added isotope solution and the in-situ dissolved Fe concentration of each sample (Measured at sea by flow injection analysis and later in the Laboratory in Kiel by standard methods [*Grasshoff et al*., 1999]). Quench curves for ^{55}Fe were produced by adding an identical amount of radiotracer and scintillation fluid to a series of samples containing a range of seawater additions.

3.4. CDOM Absorbance

[15] CDOM measurements were performed using a liquid waveguide capillary cell (LWCC) (LWCC-2100 World Precision Instruments, Sarasota, FL, USA) and an Ocean Optics USB4000 UV-VIS spectrophotometer in conjunction with an Ocean Optics DT-MINI-2-GS light source. Samples were syringe filtered through 0.2 μm filters (Sarstedt), the first 10 mL were discarded and the absorbance measured by direct injection into the LWCC. Absorbance measurements were made relative to UP water and corrected for the refractive index of seawater based on the procedure outlined in *Nelson et al.* [2007]. The resulting dimensionless optical density spectra were converted to absorption coefficient (m^{-1}): $a_{CDOM(\lambda)} = 2.303\, A_\lambda/\ell$, where 2.303 converts decadal logarithmic absorbance to base e, and ℓ is the effective optical pathlength of the waveguide (here 50.3 ± 0.5 cm as determined by the manufacturer). In the present work we

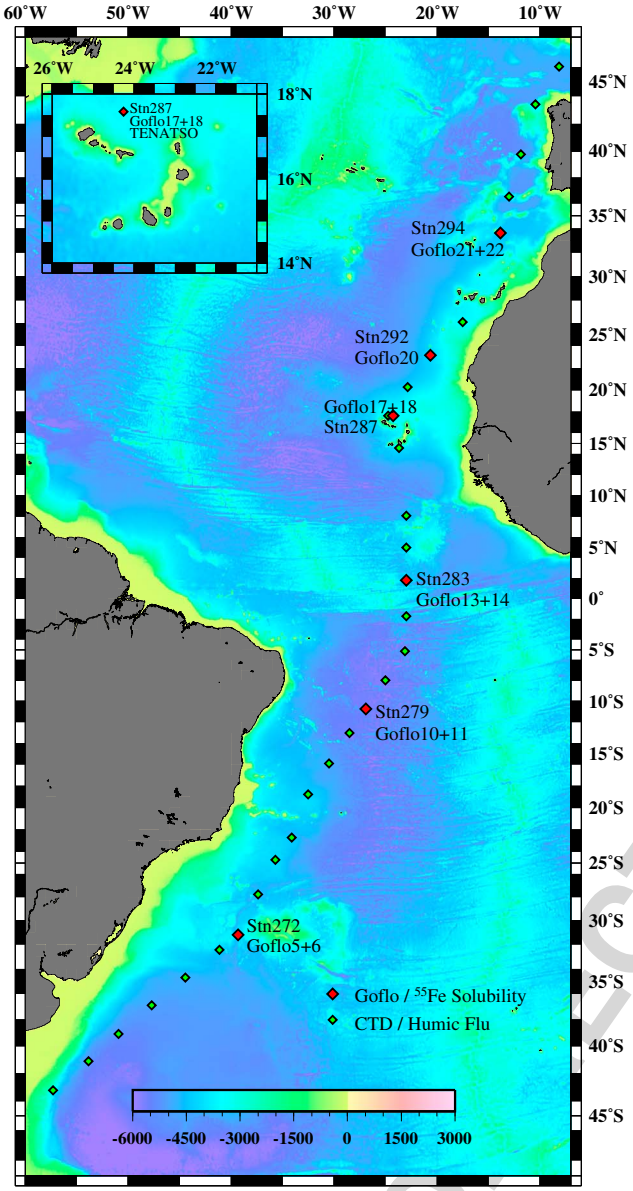

Figure 1. Station plot of the Polarstern cruise ANTXXVI-4; green diamonds show the stations where CDOM and humic Florescence measurements were made, at the stations shown as red diamonds additional Fe solubility experiments were undertaken using the radioisotope ^{55}Fe.

measured CDOM absorbance over the wavelength range 280 to 800 nm, but only the data at 325 nm (a_{325}) is presented (Figure 4). F4

3.5. Excitation Emission Matrix (EEM) and Marine Humic Fluorescence Measurements

[16] Samples for CDOM fluorescence measurements were syringe filtered through 0.2 μm filters (Sarstedt) as described above for the absorbance measurements. Humic-type fluorescence measurements were performed with a Hitachi FL-2700 Fluorometer using a 1 cm quartz cell. Measurements of HFlu [*Tani et al*., 2003] were performed by analysis of samples using excitation at 320 nm and emission at 420 nm (10 nm slit widths). Each sample was also analyzed as Excitation Emission Matrix (EEM) on the Hitachi FL-2700 Fluorometer using the same 1 cm quartz cell as for the HFlu measurements. For the EEM analysis, excitation wavelengths were scanned (12000 nm/min) from 250 to 500 nm (5 nm slit width and 5 nm increments) and emission wavelengths (5 nm slit width and 5 nm increments) from 280 to 600 nm, the photon multiplier tube (PMT) voltage was set at 700 V (maximum) and the response time 0.08 s. Sample fluorescence was normalized to daily measurements of standards of quinine fluorescence (QSU) [*Mopper and Schultz*, 1993] or to the Raman induced fluorescence of water (excitation 350 nm) [*Stedmon et al*., 2003]. The normalized EEMs were analyzed by PARAFAC in MATLAB™ under application of the DOMFluor toolbox [*Stedmon and Bro*, 2008]. Using split half analysis, four components were validated. No samples were removed from the dataset.

3.6. Dissolved Inorganic Phosphate (DIP)

[17] Samples for DIP were obtained directly from the GO-FLO bottles using the same procedure as outlined above for the iron solubility measurements and were frozen immediately for later analysis in the laboratory in Kiel. Prior to analysis samples were carefully thawed and the DIP content was detected by the method of *Murphy and Riley* [1962], with a 1 m LWCC in order to obtain the sensitivity required for detection in the nM range [*Li et al*., 2008].

3.7. H_2O_2 Measurements

[18] Samples for H_2O_2 were analysed at sea within 1–2 h of collection using a flow injection chemiluminescence (FIA-CL) reagent injection method [*Yuan and Shiller*, 1999] as described previously [*Croot et al*., 2004]. Samples were analysed using 5 replicates: typical precision was 2–3% through the concentration range 0.5–100 nM, the detection limit (3 s) is typically 0.2 nM.

4. Results and Discussion

4.1. Chlorophyll Fluorescence Along the Transect

[19] Chlorophyll fluorescence was generally low along the AMT (Figure 2) with a prominent deep chlorophyll maximum (DCM) in the oligotrophic tropical gyres as observed previously for other similar AMTs [*Tarran et al*., 2006]. There was a slight asymmetry between the Northern and Southern hemispheres as the DCM was located deeper in the south (~120–150 m) than in the north (~80–110 m). A similar asymmetry is also seen in the observed seawater temperature across the AMT with warm waters in the southern tropical gyre extending deeper than in the northern tropical gyre (Figure 3). Both of these features have been observed previously [*Tarran et al*., 2006]. F3

4.2. Iron Solubility Along the Transect

[20] Iron solubility measurements were performed at 6 stations along the AMT (Figure 1) and the iron solubility values after 48 hours for 5 of these stations (272, 279, 283, 287, 294) are shown in Figure 3. Data from station 292 were collected from only a single depth and are not discussed here. Further experiments examining the kinetics of iron solubility are presented elsewhere [*Croot and Heller*, 2012].

[21] Vertical profiles of iron solubility varied widely along the transect (Figure 3). At the southernmost station (272)

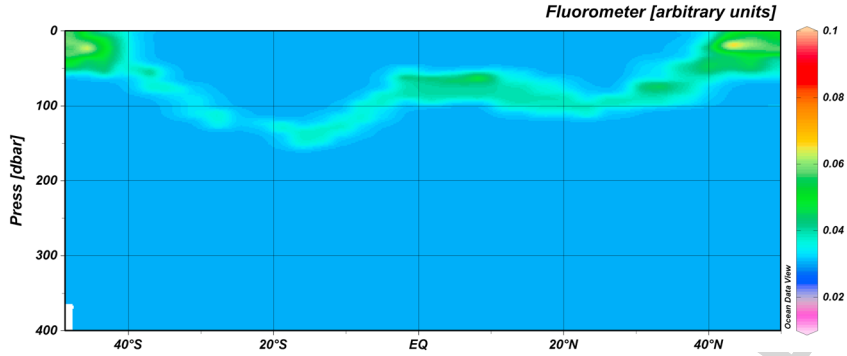

Figure 2. Plot of Chlorophyll Fluorescence during the meridional transect through the Atlantic in April–May 2010.

there was a minimum in the near-surface with a broad maximum from 40–80 m possibly related to the DCM at this location (Figure 2). At 10.7°S (Station 279) the profile decreased slightly from the surface to 200 m and then increased. Close to the equator (Station 283) the profile increased from the surface to a maximum at 100 m and was then relatively constant in the deeper waters. At the TENATSO site (Station 287) the profile was similar to that at 272 with a local maxima between 40–80 m and a gradual increase with depth. At the northern most station (294), iron solubility was relatively constant throughout the water column.

[22] The minimum in iron solubility frequently seen in the near-surface water samples is most likely related to photodegradation of iron binding ligands [*Barbeau et al.*, 2003; *Powell and Wilson-Finelli*, 2003]. The local maxima observed in the depth range 40–80 m may be related to localized production of iron complexing ligands (e.g. siderophores) by bacteria or cyanobacteria [*Ito and Butler*, 2005; *Martinez et al.*, 2001]. However the production of these ligands may not simply be related to iron limitation as a recent study has shown that siderophore production in bioassays along a similar AMT can be enhanced by the availability of different C sources [*Mawji et al.*, 2011]. Previous studies have also found that iron solubility in the open ocean is highly variable in the region between the surface and the chlorophyll maxima with both solubility minima and maxima possible [*Kuma et al.*, 1996; *Kuma et al.*, 1998; *Schlosser and Croot*, 2009].

[23] The iron solubility values we measured using the Millipore MF are much higher than those measured previously in the Atlantic with 0.02 μm Anotop filters [*Schlosser and Croot*, 2009], though they are similar to values found using the same Millipore MF filters in the North Pacific [*Kuma et al.*, 1998; *Nakabayashi et al.*, 2002] where iron solubilities up to 3.5 nM have been found in surface waters. *Chen et al.* [2004] observed that the Anotop filters were considerably different from their rated pore size of 0.02 μm (or ~500 kDa; Chen et al. state 2000 kDa in their work but most manufacturers of 20 nm filters indicate it is nominally 500 kDa) as their own investigations indicated it was actually ~3 kDa, this is also in line with work performed in our own laboratory (C. Schlosser, submitted to *Limnology and Oceanography Methods*). The 0.025 μm Millipore MF filters used in the present study appear to have a filter cutoff more in keeping with their stated poresize based on comparison with ultrafiltration (P. Croot, unpublished data). Another important difference between our work and earlier studies is that our samples were processed immediately at sea, while other studies were performed on samples that had been frozen and then later thawed in the laboratory. Recent work has shown that freezing of samples can impact iron

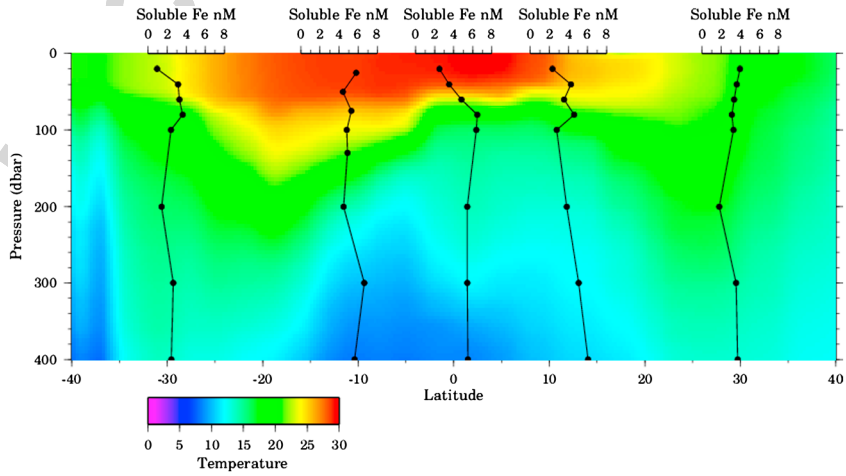

Figure 3. Distribution of temperature along the meridional transect in the Atlantic. Superimposed over the transect is the soluble Fe concentrations at each station measured along the transect.

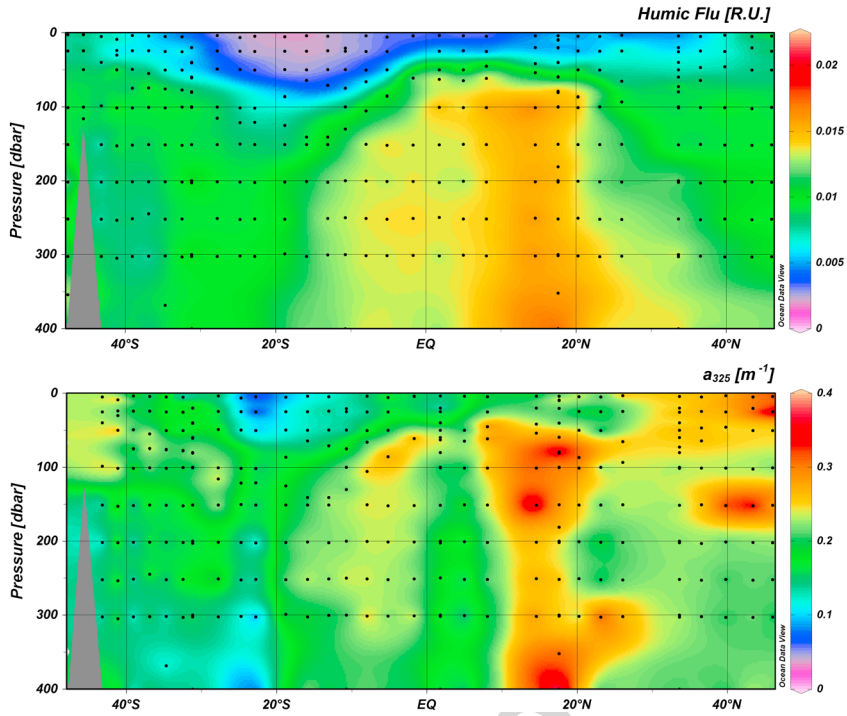

Figure 4. (4A-upper panel) Marine humic fluorescence (320 nm excitation, 420 nm emission) across the meridional transect in the Atlantic Ocean; (4B–lower panel) The distribution of CDOM absorbance at 325 nm (a_{325}) along the AMT is shown in Figure 4B.

solubility measurements performed by using Anotop filters [*Schlosser et al*., 2011] and presumably this may also apply to other filters.

[24] The cutoff used in pre-filtration of the water sample may also have an impact on the results of the iron solubility experiments, as studies using 0.45 μm pre-filtration [*Kuma et al*., 1996; *Liu and Millero*, 2002] have shown that equilibrium is established over timescales ranging from 1–2 weeks, while less than 24 hours was required when 0.2 μm pre-filtration was used [*Chen et al*., 2004]. The results of *Chen et al.* [2004] agree with kinetic experiments we performed during this cruise [*Croot and Heller*, 2012] as we observed that there was relatively little change in iron solubility after 24 hours using 0.2 μm pre-filtration. Thus the inclusion of significant colloidal matter/ligands may have an important influence on the kinetics and final equilibrium value of iron solubility attained. Additionally adsorption to the walls of the sample containers may also be a critical factor [*Fischer et al*., 2007; *Schlosser et al*., 2011]. In the present work we used Teflon throughout, while earlier studies have used both polypropylene [*Kuma et al*., 1996; *Nakabayashi et al*., 2002] and also Teflon [*Liu and Millero*, 2002]. Kinetics here are also important as longer incubation times may lead to a greater degree of wall adsorption [*Schlosser et al*., 2011].

[25] Iron complexation studies, typically using voltammetric methods [*Croot and Johansson*, 2000; *Rue and Bruland*, 1995], have indicated that iron in surface waters is strongly complexed by organic ligands. The presumption is that these same ligands are responsible for elevating iron solubility above the ~80 pM limit imposed by the low solubility of inorganic iron [*Liu and Millero*, 2002]. It is important to note here that the voltammetric methods don't measure the total iron binding ligand concentration present in seawater but an operational defined fraction that is detectable through competition with an added ligand at a given detection window. Thus in general voltammetric methods should determine a lower value than iron solubility methods when using the same filtration cutoff. In practice however voltammetric measurements are performed on 0.2 μm filtered water and thus still include colloids [*Boye et al*., 2010].

[26] There has been only a handful of iron speciation studies reported along the here presented AMT. The earliest study was performed in the south and equatorial Atlantic and found that there was no systematic variation in ligand concentrations (1–2 nM) with either depth or water mass, with an excess of ligands in near surface waters [*Powell and Donat*, 2001]. Studies in the oligotrophic Canary basin [*Gerringa et al*., 2006] found relatively low Fe concentrations whereas Fe complexing ligands abounded especially in the mixed layer. Some phytoplankton groups (*Synechococcus* and pico-eukaryotes) were positively correlated with iron binding ligand concentrations and *Gerringa et al.* [2006] suggested, that these groups may be partly responsible for ligand production, however the relationship was not statistically significant due to the small sample size (n = 4). These authors further suggested that organic compounds leaking out of non-viable cells [*Veldhuis et al*., 2001], possibly via viral lysis of cells [*Poorvin et al*., 2011], in the surface waters could act as ligands in addition to the active production of siderophores in response to iron stress. A similar hypothesis has been put forward for Cu ligands in seawater [*Croot et al*., 2000].

[27] A more recent iron speciation study in the NE Atlantic Ocean, adjacent to Cape Verde, at a time when surface concentration of dissolved iron were low (0.1–0.4 nM) also found higher concentrations of ligands (0.82–1.46 nM) with

a high percentage of uncomplexed ligands [*Rijkenberg et al*., 2008]. These workers were able to samples both before and after a relatively small Saharan dust event and observed a small increase in dissolved iron (0.2 to 0.25 nM) and a decrease in the concentration of uncomplexed iron binding ligands (1.15 to 0.89 nM), coupled with no detectable change in the stability constant for the ligands after the dust event. This suggested to those authors that there was no further input of Fe binding ligands either from dust deposition or in the biotic response to this event.

[28] The identification of distinct iron binding ligands in seawater is in its infancy. In a pioneering study a number of hydroxamate siderophores were identified at the pM level along an AMT, May–June 2005, from South Africa to the UK [*Mawji et al*., 2008]. Ferrioxamine G was found throughout the transect (2.6–10.5 pM) with lowest concentrations in the oligotrophic gyres. Ferrioxamine E was only found in the sub–tropical and temperate regions (0.1–10.2 pM) and was below detection (<0.1 pM) in the equatorial and oligotrophic gyre regions. Amphibactin siderophores were below detection throughout the AMT but were detected along with Ferrioxamines E and G in samples enriched with glucose, nitrate and phosphate. Both the Amphibactins and Ferrioxamine G are produced by marine *Vibrio* species [*Martinez et al*., 2001; *Martinez et al*., 2003], which are ubiquitous throughout this region and are believed to be growth limited by DOC rather than other nutrients [*Neogi et al*., 2011]. Overall this indicates that while if there is a link between DOC and the production of siderophores, the actual components involved directly do not contribute significantly to either the CDOM absorbance or fluorescence of the bulk seawater. Thus any correlation between iron solubility and CDOM is due to other organic components that are produced by related processes.

4.3. Distribution of Marine Humic Fluorescence in the Upper 400 m

[29] Discrete measurements of HFlu (Ex 320/Em 420) along the AMT are shown in Figure 4A. A key feature to note is that HFlu increases with depth right across the transect with very low values (≤0.0023–0.0069 RU) in surface waters between 40°S and 40°N. There was a well-developed minima in the southern tropical gyre (5°–30°S) which extended from the surface to ~100 m, and apparently tracked immediately above the location of the DCM in this region (Figure 2). A strong maximum was seen in the depth range 100–400 m from 5°S to 20°N and appeared to be related to the oxygen minimum zone (OMZ) located here [*Stramma et al*., 2009]. This would be consistent with data from the Pacific that found a strong correlation between HFlu and AOU [*Hayase and Shinozuka*, 1995; *Kuma et al*., 1998; *Yamashita et al*., 2007].

4.4. CDOM Absorbance

[30] The distribution of CDOM absorbance (325 nm, a_{325}) along the AMT is shown in Figure 4B. The main feature to note is the high values of a_{325} (up to 0.4 m^{-1}) found at depth in the vicinity of the Cape Verde Islands (15–20°N). In general, similar to the humic fluorescence, values of a_{325} in the surface waters are low in the equatorial and tropical regions and increase pole wards. Results from other AMT's [*Kitidis et al*., 2006] also indicate maximum for a_{300} (up to 0.6 m^{-1}) centered around 10°N and is most likely related to the OMZ present there [*Stramma et al*., 2009] and the remineralization of organic matter. Our data is broadly comparable with the recently published data of *Nelson et al*. [2010], though we don't observe the strong north-south asymmetry that they report. This is mostly likely because in the region of 10–20°N our data is influenced by proximity to the Cape Verde islands and their data is a composite containing lower CDOM regions in the oligotrophic western Atlantic.

4.5. Humic Fluorescence–Unit Conversion–Comparison with Pacific Studies

[31] In the present work we chose to use Raman units (RU) for reporting our fluorescence data as this removes instrument-dependent intensity factors, and allows the presentation of results on a unified scale [*Lawaetz and Stedmon*, 2009]. Previously workers in this field have most commonly utilized quinine sulfate as a fluorescence standard and reported intensities as quinine sulfate units ($QSU_{ex/em}$) at specific excitation and emission wavelengths, and so in the present work we also developed calibrations using two common QSU sets so that they could be inter-compared (Table S1)[1]. We found excellent agreement with the earlier results of *Lawaetz and Stedmon* [2009] for the relationship between $QSU_{350/450}$ and RU indicating the robustness of this approach as the values were obtained on different fluorometers. We also found that there was no statistically significant difference between the conversion values when different slit width combinations were used (Table S1). Excellent agreement was also seen for intensity values measured with different slit widths (Figure S1) as in the present case we could also extract the intensity values for HFlu from the independently run EEM measurements which utilized smaller slit widths.

[32] Using the conversion factors shown in Table S1, the maximum $QSU_{320/420}$ was found to be 1.71 along our AMT with an average of 0.80 ± 0.34 (1σ) over the entire data set (n = 366). This compares with values ranging from 0 to 2.5 $QSU_{320/420}$ for a meridional transect in the North Pacific [*Yamashita and Tanoue*, 2009]. In that study the distribution of HFlu in the upper 500 m had some similarities to the present work as lowest values of HFlu were found in the surface waters of the oligotrophic tropical gyre and a local maxima was found at ~100 under this surface minima. Highest values of HFlu, $QSU_{320/420} > 2$, were found in North Pacific intermediate water (NPIW) and these authors suggested that this was due to the contribution of riverine input to the source regions for NPIW, the Sea of Okhotsk and the Gulf of Alaska. In this study we did not encounter any water masses formed in regions of high freshwater input; as the rivers are minor sources along the Patagonian shelf [*Gaiero et al*., 2003; *Scapini et al*., 2010], and the ships track was far from the Amazon plume and there are no major riverine sources in the Tropical Eastern Atlantic [*Cotrim da Cunha et al*., 2009].

4.6. CDOM Fluorescence - PARAFAC Components

[33] PARAFAC analysis of the EEMs found 4 distinct components (C1–C4) and their distribution along the AMT

[1]Auxiliary materials are available in the HTML. doi:10.1002/gbc.20004.

is shown in Figure 5. The resulting EEMs for C1-C4 are also shown in Figure S2 and summarized in Table 1. Highest fluorescence intensities were found for C1 and the lowest for C4; All values in RU ($\pm 1\sigma$): C1 0.073 ± 0.033, max 0.239, C2 0.027 ± 0.009, max 0.054, C3 0.034 ± 0.023, max 0.247, C4 0.010 ± 0.005, max 0.021. The EEMs for C1 and C3 are similar to that found for pure solutions of Tyrosine and Tryptophan in seawater (Table 1), respectively [*Yamashita and Tanoue*, 2003b] and have been identified in previous open ocean studies [*Coble*, 1996; *Jørgensen et al*., 2011; *Murphy et al.*, 2010]. Similarly C2 and C4 were similar (Table 1) to marine or terrestrial humics [*Coble*, 1996; *Jørgensen et al*., 2011; *Murphy et al.*, 2010]. Indeed C4 was strongly correlated (R = 0.95, Table 2) to the independent measurements of humic fluorescence suggesting that these components were identical.

[34] A recent study used the relationship between the fluorescence of Tyrosine and Tryptophan to determine apparent concentrations of these amino acids in seawater. In the present work we did not directly attempt to calibrate the signals for C1 and C3 in terms of the Tyrosine and Tryptophan concentrations, but can estimate their concentrations by using the relationship found earlier by *Jørgensen et al*. [2011]. Using this approach we estimate that the mean concentrations of Tyrosine and Tryptophan over our study area was 5.9 ± 2.6 nM and 2.8 ± 1.9 nM respectively. This is significantly lower than the mean concentrations for the upper 100 m found by *Jørgensen et al.* [2011] using PARAFAC analysis (Trypotphan 12.5 nM and Tyrosine 15.8 nM). The most likely reason for this difference is that the Jørgensen et al. work included more near shore environments and less open ocean sites than our work. Other estimates for Tyrosine concentrations along an AMT have been made using concentration series bioassays with radiolabelled free Tyrosine [*Zubkov et al.*, 2008] and indicate much lower concentrations 0.16 ± 0.11 nM in the Gyres, 0.65 ± 0.57 nM in the Equatorial region. This strongly suggest that the fluorometric approach is also measuring protein bound Tyrosine. This is partly confirmed by comparing with measurements of Tyrosine in bulk DOM from the North Pacific [*Yamashita and Tanoue*, 2003a]. The range values found in surface waters (of 2.1–5.9 nM) is in mid-depth waters (2.0–5.3 nM) very similar to our estimates for the Atlantic.

[35] A particular feature to note in our data is the maximum in C1 in the upper 100 m of the oligotrophic southern tropical gyre (Figure 5). This maximum in C1 (equivalent to 8–12 nM Tyrosine–see above) was found in the euphotic zone above the DCM (Figure 2) and in the region of the low humic fluorescence (Figure 4). The southern gyre is strongly iron limited resulting in lower N_2 fixation than in the northern gyre which receives iron via deposition of Saharan dust [*Moore et al*., 2009]. The reasons why Tyrosine would be present in higher concentrations in the southern gyre are not clear as it is a bioavailable source of DOC and DON for bacteria with free Tyrosine utilized rapidly [*Zubkov et al*., 2008].

[36] The tryptophan like component, C3, had low concentrations in the south with higher values found in the north, there was a weak but significant correlation with chlorophyll fluorescence (Table 2). *Determann and coworkers* [1994; 1998] have shown previously that phytoplankton and bacteria are sources for tryptophan and tyrosine. Direct measurements of tryptophan in the open ocean are only available for the North Pacific with values of 0.3–1.6 nM in the surface waters and 0.5–1.6 nM in mid-depth waters [*Yamashita and Tanoue*, 2003a], which are slightly lower than our estimates for the Atlantic. A feature of our results (Figure 5) was the high variability particularly in the region 15°–40°N. High variability in the tryptophan fluorescence signal below the mixed layer was also previously seen with unfiltered samples from the Tropical Eastern Atlantic Ocean [*Determann et al*., 1996] which they ascribed to tryptophan bound to bacteria. In the present work we saw considerable variability with 0.2 μm filtered seawater which excludes bacteria and thus an alternate explanation is required. One possibility is that the dissolved tryptophan 'hotspots' we observed are related to zooplankton grazing where particulate tryptophan is converted into soluble and colloidal phases. However we note also that the production of tryptophan by grazing may be influenced by the size of the grazer, as tryptophan is easily hydrolysed to pyruvate and indole at low pH, passage through the low pH of protozoan grazers [*Fok et al*., 1982] may result in the loss of tryptophan.

[37] For the humic-like components C2 and C4 (Figure 5) no specific chemical species has been identified, but that the fluorescence represents a range of compounds [*Boyle et al*., 2009; *Ma et al*., 2010]. As mentioned above the C4 component was strongly correlated with measurements of HFlu (Table 2) and thus the distribution of the two parameters are almost identical (Figures 4 and 5). The C2 component showed quasi symmetry at the equator (Figure 5) with maxima at 10°S and 15°N, this humic like (Table 1) component was otherwise relatively uniform throughout the transect. Over the complete dataset C2 was weakly positively correlated with depth (Table 2), however there was wide variability between individual CTD profiles along the AMT and no clear trend with water mass or biogeochemical province was discernible. A component showing similarity to C2 was recently reported as being produced from the photochemical irradiation of refractory DOM in the Baltic [*Karl et al*., 2012] and was also observed in the Pacific and the Atlantic [*Jørgensen et al*., 2011; *Murphy et al.*, 2008]. It was suggested by *Murphy et al.* [2008] that this component is a long-lived product of the photodegradation of organic matter. However recent work also suggests a component like C2 may be produced directly by marine bacteria [*Shimotori et al*., 2012].

[38] The CDOM absorbance at 325 nm was weakly correlated with C2, C3, and C4 (Table 2), indicating that the bulk of the CDOM absorbance was not related to the fluorometric signal. Earlier studies have found strong correlations between humic fluorescence and a_{320} [*Yamashita and Tanoue*, 2009] in deep waters with the correlation becoming weaker in surface waters.

4.7. Relationship Between CDOM and Nutrients

[39] DIP was not significantly correlated with either CDOM absorbance, a_{325}, or the protein-like fluorescent components C1 and C3 in this work (Table 2). Most of the studies which have previously found a positive correlation between CDOM absorbance and nutrients were conducted in the Pacific Ocean and significant relationships were only found in deep and intermediate waters below the surface mixed layer. The recent global study by *Nelson et al.* [2010] indicated a significant positive correlation between CDOM and organic matter remineralization for the Pacific, Indian and Atlantic

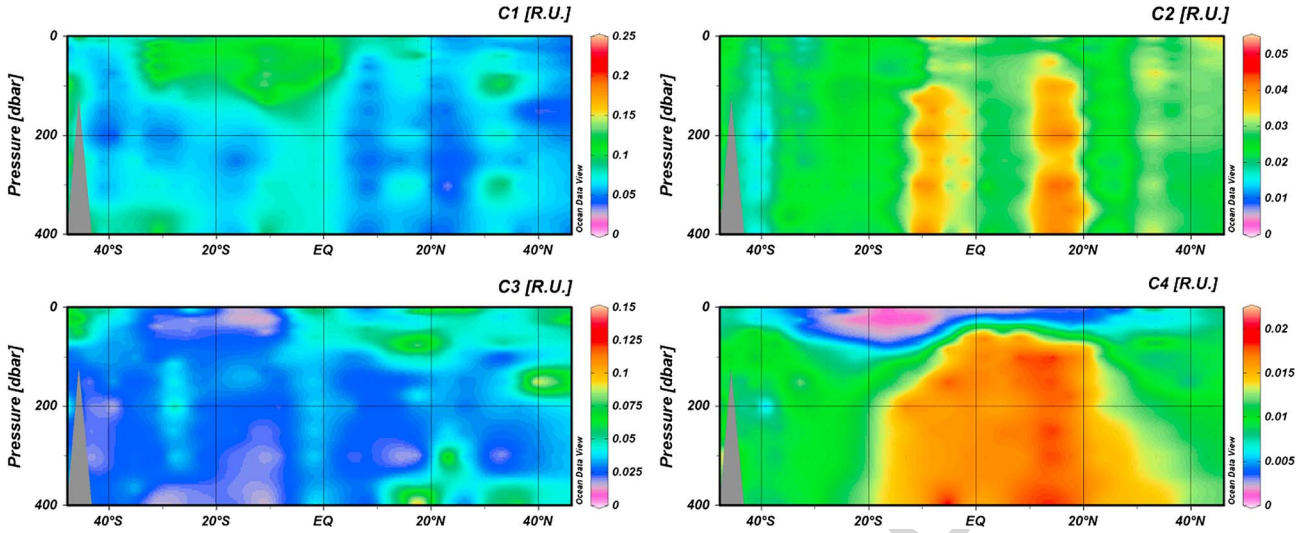

Figure 5. Distribution of the four components which result from the PARAFAC modeling of the data set; the (top left, C1) Component 1: Tyrosine- or protein-like peak; (top right, C2) Component 2: Terrestrial Humic Substance 'A' or humic like peak; (below left, C3) Component 3: Tryptophan- like peak 'T' or amino acids and (below right, C4) Component 4: Marine fulvic 'M', UV/ Visible humic-like or Marine humic material.

Ocean. However a closer look at their data shows that the R^2 for the correlation with DIP in the Pacific and Indian are 0.77 and 0.66 respectively whereas for the Atlantic a R^2 of only 0.11 is presented in line with our own work.

[40] However significant weak correlations (R = 0.35–0.49) were found between DIP and the humic components C2, C4, and the direct measurements of humic fluorescence. These findings are in line with previous studies which have shown that humic fluorescence was strongly correlated with nutrients (NO_3^-, PO_4^{3-}) in different intermediate and deep water masses [*Hayase and Shinozuka*, 1995; *Jørgensen et al.*, 2011; *Yamashita and Tanoue*, 2008; *Yamashita et al.*, 2007], these authors have used these correlations to suggest that humic fluorescent organic matter is regenerated in the water column by oxidation and remineralization of organic substances in sinking particles.

4.8. Distribution of H_2O_2

[41] The mid-day distribution of H_2O_2 along the AMT is shown in Figure 6. H_2O_2 was relatively constant in the upper 50 m and decreased rapidly below the mixed layer, with low concentrations (<5 nM) found below the euphotic zone. Our results are consistent with previous data from this region [*Croot et al.*, 2004; *Heller and Croot*, 2010b; *Steigenberger and Croot*, 2008; *Yuan and Shiller*, 2001]. Surface concentrations were elevated in the region between 25°and 40°N and this was most likely due to a combination of clear skies and the season (i.e. longer irradiation time between dusk and local midday at these locations in spring/summer). The H_2O_2 signal in surface waters is impacted by a strong diel signal induced by the solar cycle. Estimates for the strength of this diel cycle in the open Atlantic range from 25 to 50 nM [*Croot et al.*, 2011; *Yuan and Shiller*, 2001]. By sampling at local noon we do not observe the local maxima for H_2O_2 which typically occurs in the afternoon or early evening [*Yuan and Shiller*, 2001]. However by the use of a common time point for sampling it provides a valid comparison between stations along the AMT so that the general trends in H_2O_2 may be observed.

4.9. Possible Impact of Irradiation on H_2O_2 and CDOM Properties

[42] In order to examine the possible impact of solar irradiation on CDOM properties over the AMT we analyzed our data using depth (pressure) as a proxy for the irradiance

Table 1. Humic Fluorescence Components

Component ex/em	Fluorescence Characteristics ex/em	Description and probable source
C1 280/310	275/305	Tyrosine-like peak 'B' [*Coble*, 1996][a]
	280/305	'BT' protein-like [*Wedborg et al.*, 2007][b]
	280/310	Tyrosine 'C5' [*Jørgensen et al.*, 2011][b]
C2 250/475	<260/400–460	Terrestrial Humic Substance 'A' peak [*Coble*, 1996][a] Humic like [*Dubnick et al.*, 2010][b] Humic like 'C1' [*Jørgensen et al.*, 2011][b]
C3 280/320	275/340	Tryptophan-like peak 'T' [*Coble*, 1996][a]
	280/328	Amino acids 'C6' [*Murphy et al.*, 2010][b]
	280/330	Tryptophan 'C2' [*Jørgensen et al.*, 2011][b]
C4 335/400	290–310/ 370–410	Marine fulvic 'M' peak [*Coble*, 1996][a]
	340/420	UV/Visible humic-like [*Wedborg t al.*, 2007][b]
	315/418	Marine humic material 'C2'[*Murphy et al.*, 2010][b]

Notes:
[a]Manual EEM interpretation.
[b]PARAFAC analysis.

Table 2. Results of Spearman Rank Analysis of Correlations (ρ) between the Parameters Measured in this Study.

	Lat	Long	Press	Temp	Salt	AFL	Hflu	SolFe	DIP	a325	C1	C2	C3	C4	H_2O_2
Lat	1.00	**0.95**	−0.01	0.07	**0.29**	**−0.45**	**0.21**	0.13	0.35	**0.29**	**−0.21**	**0.30**	**0.29**	**0.20**	0.10
Long		1.00	0.02	0.04	**0.34**	**−0.45**	**0.24**	0.04	0.23	**0.34**	**−0.23**	**0.35**	**0.26**	**0.21**	0.07
Pressure			1.00	**−0.63**	**−0.35**	**−0.20**	**0.68**	0.28	**0.84**	0.08	**−0.17**	**0.10**	**−0.37**	**0.67**	**−0.76**
Temp				1.00	**0.76**	**−0.21**	**−0.60**	–	–	**−0.26**	**0.22**	**−0.13**	**0.24**	**−0.56**	**0.68**
Salt					1.00	**−0.31**	**−0.42**	–	–	**−0.14**	0.06	−0.06	**0.21**	**−0.41**	**0.52**
AFL						1.00	−0.02	–	–	**0.39**	**−0.16**	0.06	**0.52**	−0.04	**0.37**
Hflu							1.00	0.06	**0.71**	**0.49**	**−0.25**	**0.36**	−0.07	**0.95**	**−0.52**
SolFe								1.00	**0.59**	0.05	−0.07	0.18	−0.02	0.21	–
DIP									1.00	0.07	−0.54	**0.64**	0.05	**0.77**	–
a325										1.00	−0.22	**0.35**	**0.27**	**0.45**	−0.06
C1											1.00	**0.27**	**−0.30**	**−0.28**	0.18
C2												1.00	−0.01	**0.32**	−0.03
C3													1.00	−0.06	**0.32**
C4														1.00	**−0.52**
H_2O_2															1.00

Notes: Spearman rank Correlation analysis was performed pairwise using the corr function in Matlab™. Analysis was performed on the entire dataset. Continuous parameters from the CTD included; Latitude (Lat, n = 958), longitude (Long, n = 958), pressure (Press, n = 958), temperature (Temp, n = 918), salinity (Salt, n = 918), chlorophyll fluorescence (AFL, n = 378). Other data was obtained via discrete sampling from the CTD rosette or GO-FLOs; humic fluorescence (Hflu, n = 366), CDOM absorbance (a325, n = 355), PARAFAC derived components C1–C4 (n = 368) and H_2O_2 (n = 301). Dissolved inorganic phosphorous (DIP, n = 32) and the iron solubility (SolFe, n = 40) were determined only from GO-FLO bottles, which were not equipped with temperature, salinity, or chlorophyll fluorescence sensors, so no data pairs exist for these analyses (marked above as -). Values in bold indicate the correlation is significant at the $p < 0.001$ level.

field. H_2O_2 which is predominantly photochemically produced, typically strongly correlated with irradiance [*Steigenberger and Croot*, 2008], was significantly negatively correlated with pressure (Table 2) as would be expected for a photo-produced species. Positive correlations would be expected for substances that are photo-bleached. Humic fluorescence and C4 were significantly positively correlated with pressure (Table 2), while C2 was only weakly correlated (R = 0.10). However CDOM absorbance, a_{325}, over the entire dataset (0–400 m) was not significantly correlated with depth. Part of the reason for the poor correlation overall is due in part to the inclusion of data from below the euphotic zone, where the impacts of irradiation are not expected. Limiting the dataset to solely the euphotic zone, approximated at 100 m based on the both the location of the DCM (Figure 2) and the H_2O_2−cline (Figure 5), improved the overall correlation only slightly (CTD only, R = 0.25, n = 136, GO-FLO only, R = 0.36, n = 20).

[43] Light absorption by CDOM initiates photochemical reactions resulting in loss of CDOM absorption or photobleaching and in the production of a variety of photoproducts such as $O_2^-$and ultimately H_2O_2 [*Heller and Croot*, 2010a; *O'Sullivan et al*., 2005]. Photobleaching in surface waters has been observed at TENATSO previously [*Heller and Croot*, 2010b] as evidenced by decreases in a_{325} values from depth towards the surface, and was evident again at this site (S287, data not shown) but was not prevalent over the entire AMT. H_2O_2 was significantly negatively weakly correlated with C4/humic fluorescence suggesting that this component is possibly a better proxy for the primary chromophore for H_2O_2 than CDOM absorbance.

4.10. Relationship Between Humic Fluorescence and Iron Solubility

[44] In the present study iron solubility was found to be only significantly correlated with DIP (R = 0.59, Table 2) and it was poorly correlated with HFlu or any of the humic-like components (C2, C4) (Figure 5) identified by PARAFAC analysis. Previous work has shown strong correlations between HFlu and iron solubility for intermediate and deep waters with weak or no-correlation in the surface waters [*Kuma et al*., 1998; *Nakabayashi et al*., 2001; *Nakabayashi et al*., 2002; *Tani et al*., 2003]. Figure S3 shows clearly the lack of any general relationship between HFlu and iron solubility for this study. However examination of individual stations reveals that at different locations significant linear relationships do exist; in the entire water column at Station

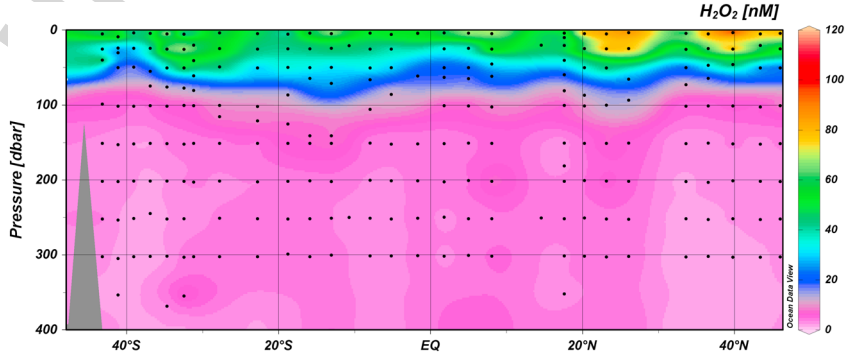

Figure 6. Section showing the mid-day distribution of H_2O_2 in nM in the water column along the meridional transect in the Atlantic Ocean.

283 (R = 0.87, n = 8) and from 80 to 400 m at Station 287 (R = 0.6, n = 5). Both of these stations lie in the region of the high dust deposition from the Sahara and the OMZ.

[45] The HFlu (Figure 4A) maxima in the waters below the euphotic zone in this region suggests strong remineralization, as evidenced by high AOU and N_2O [*Forster et al*., 2009]. The high dust inputs to this region suggest that this region is likely to be Fe replete for phytoplankton and bacteria and that these organisms are likely nitrogen or DOC limited respectively. Thus here it is unlikely that there is considerable siderophore production in response to iron stress and thus Fe solubility is dominated by the presence of ligands produced by remineralization processes [*Boyd et al*., 2010; *Schlosser et al*., 2012]. In the Fe deplete regions encountered during this AMT production of siderophores in response to Fe stress was likely a key control on Fe solubility and this distorted any relationship with HFlu.

[46] Our data suggests then that there is no simple global relationship between iron solubility and any of the CDOM parameters in surface waters. Previous studies have shown relationships between DOC and iron solubility [*Chen et al*., 2004] and DOC and iron complexing ligands [*Wagener et al*., 2008]. The relationships found in these studies have been subsequently been incorporated by modelers [*Tagliabue and Völker*, 2011] into parameterizations for iron binding ligand concentrations in global models as DOC already exists as a key parameter. Further work though is clearly needed over a range of ocean environments to check the validity of these parameterizations.

[47] Recent work has suggested that humics form strong complexes with iron in seawater and that they could account for the entire ligand concentration in both shallow coastal and deep ocean waters, though no vertical profiles were reported [*Laglera and van den Berg*, 2009]. The analytical method they used [*Laglera et al*., 2007] is similar to the solubility work presented here in its initial steps as they add Fe to saturate all the ligands and then later measure by voltammetry a catalytic reduction current in the presence of bromated for the Fe-humic complexes formed. Thus based on their findings we would expect better correlations between humic fluorescence and iron solubility in our work than we observed. We note that similar work on quantifying humics by Quentel and coworkers [*Chanudet et al*., 2006; 1987], using molybdate, showed it was purely a surface reaction and not related to the bulk concentration of the molybdate-humic complex. Our suspicion is then that the Fe-humic response is also predominantly a surface process, and is not specific to humics *per se*, as evidenced by enhanced 'humic' concentrations on addition of surface active carbohydrates [*Hassler et al*., 2011]. Additionally our related kinetic work [*Croot and Heller*, 2012] would indicate that thermodynamically weak ligands would also contribute to the iron humic signal leading to an overestimation of the concentration of ligands that can stabilize Fe in solution. A clear goal of future work then is a comparison between these different measurements of humics and humic iron binding in seawater and their distributions in order to better understand what is being assayed.

5. Conclusions

[48] That iron binding organic ligands are critical to determining Fe solubility in the surface ocean is not in doubt. However from the data collected here across an AMT it is not possible to provide a simple global parameterization for this as iron solubility was only weakly correlated with DIP and it was poorly correlated with any of the humic-like components (C2, C4) identified by PARAFAC analysis. It appears that while significant correlations with humic-like components may exist in iron-replete regions, in iron-deplete regions the production of specific iron binding compounds in surface waters is not related to any of the properties of bulk CDOM. The humic fluorescence signal was sharply attenuated in surface waters, presumably due to photo bleaching, but this was only poorly correlated to the transient photo produced species, H_2O_2, most likely due to the different lifetimes of these compounds in the ocean.

[49] This study makes important contributions towards our understanding of the biogeochemical cycling of iron and CDOM in the open ocean and especially in the poorly studied South Atlantic Ocean. More measurements of iron solubility over a range of temporal and spatial scales is clearly required if we are to better understand what are the controls on this important property of iron chemistry in seawater and we hope that this study will spur others to make such measurements. Further work is also needed on the links between the different measure of humic abundance and how they relate to other biogeochemical processes in the ocean.

[50] **Acknowledgments.** The authors would like to express their deep thanks and appreciation to the captain and crew of the R.V. Polarstern (ANTXXVI-4). We are indebted to Dr Thibaut Wagener and Ms Mirja Dunker for the DIP data. This work was financially supported by grants awarded to PLC; DFG project ADIOS-BAO (CR145/18-1) and as part of the BMBF Verbundsprojekt SOPRAN II (IG03). This work is also a contribution to German SOLAS (SOPRAN).

References

Amador, J., P. J. Milne, C. A. Moore, and R. G. Zika (1990), Extraction of chromophoric humic substances from seawater, *Mar. Chem.*, *29*, 1–17.

Aristegui, J., C. M. Duarte, S. Agusti, M. Doval, X. A. Alvarez-Salgado, and D. A. Hansell (2002), Dissolved organic carbon support of respiration in the dark ocean, *Science*, *298*(5600), 1967–1967.

Baker, A. R., and P. L. Croot (2010), Atmospheric and marine controls on aerosol iron solubility in seawater, *Mar. Chem.*, *120*, 4–13.

Barbeau, K., E. L. Rue, C. G. Trick, K. W. Bruland, and A. Butler (2003), Photochemical reactivity of siderophores produced by marine heterotrophic bacteria and cyanobacteria based on characteristic Fe(III) binding groups, *Limnol. Oceanogr.*, *48*, 1069–1078.

Boreen, A. L., B. L. Edhlund, J. B. Cotner, and K. McNeill (2008), Indirect Photodegradation of Dissolved Free Amino Acids: The Contribution of Singlet Oxygen and the Differential Reactivity of DOM from Various Sources, *Environ. Sci. Technol.*, *42*(15), 5492–5498.

Boyd, P. W., E. Ibisanmi, S. G. Sander, K. A. Hunter, and G. A. Jackson (2010), Remineralization of upper ocean particles: Implications for iron biogeochemistry, *Limnol. Oceanogr.*, *55*(3), 1271–1288.

Boye, M., J. Nishioka, P. Croot, P. Laan, K. R. Timmermans, V. H. Strass, S. Takeda, and H. J. W. de Baar (2010), Significant portion of dissolved organic Fe complexes in fact is Fe colloids, *Mar. Chem.*, *122*(1–4), 20–27.

Boyle, E. S., N. Guerriero, A. Thiallet, R. Del Vecchio, and N. V. Blough (2009), Optical Properties of Humic Substances and CDOM: Relation to Structure, *Environ. Sci. Technol.*, *43*(7), 2262–2268.

Chanudet, V., M. Filella, and F. Quentel (2006), Application of a simple voltammetric method to the determination of refractory organic substances in freshwaters, *Anal. Chim. Acta*, *569*(1–2), 244–249.

Chen, M., W. X. Wang, and L. D. Guo (2004), Phase partitioning and solubility of iron in natural seawater controlled by dissolved organic matter, *Global Biogeochem. Cycles*, *18*(4).

Coble, P. G. (1996), Characterization of marine and terrestrial DOM in seawater using excitation emission matrix spectroscopy, *Mar. Chem.*, *51*(4), 325–346.

Coble, P. G. (2007), Marine Optical Biogeochemistry: The Chemistry of Ocean Color, *Chem. Rev.*, *107*(2), 402–418.

Cooper, W. J., R. G. Zika, R. G. Petasne, and A. M. Fischer (1988), Sunlight-Induced Photochemistry of Humic Substances in Natural Waters: Major Reactive Species, in Aquatic Humic Substances, edited, pp. 333–362, American Chemical Society.

Cotrim da Cunha, L., P. Croot, and J. LaRoche (2009), Influence of river discharge in the tropical and subtropical North Atlantic Ocean, *Limnol. Oceanogr.*, *54*(2), 644–648.

Croot, P. L., and M. Johansson (2000), Determination of iron speciation by cathodic stripping voltammetry in seawater using the competing ligand 2-(2-Thiazolylazo)-p-cresol (TAC), *Electroanalysis*, *12*(8), 565–576.

Croot, P. L., and M. I. Heller (2012), The importance of kinetics and redox in the biogeochemical cycling of iron in the surface ocean, *Front. Microbiol.*, *3*, doi:10.3389/fmicb.2012.00219.

Croot, P. L., J. W. Moffett, and L. Brand (2000), Production of extracellular Cu complexing ligands by eucaryotic phytoplankton in response to Cu stress, *Limnol. Oceanogr.*, *45*, 619–627.

Croot, P. L., K. Bluhm, M. I. Heller, and K. Wuttig (2011), Transient redox species as tracers of oceanographic mixing and transport, *J. Mar. Syst.*, (submitted).

Croot, P. L., P. Streu, I. Peeken, K. Lochte, and A. R. Baker (2004), Influence of the ITCZ on H_2O_2 in near surface waters in the equatorial Atlantic Ocean, *Geophys. Res. Lett.*, *31*, L23S04, doi:10.1029/2004GL020154.

Determann, S., R. Reuter, and R. Willkomm (1996), Fluorescent matter in the eastern Atlantic Ocean. Part 2: vertical profiles and relation to water masses, *Deep-Sea Res. Pt I*, *43*(3), 345–360.

Determann, S., R. Reuter, P. Wagner, and R. Willkomm (1994), Fluorescent Matter in the Early Atlantic-Ocean. 1. Method of Measurement and near-Surface Distribution, *Deep-Sea Res. Pt I*, *41*(4), 659–675.

Determann, S., J. M. Lobbes, R. Reuter, and J. Rullkötter (1998), Ultraviolet fluorescence excitation and emission spectroscopy of marine algae and bacteria, *Mar. Chem.*, *62*(1–2), 137–156.

Evangelista, H., et al. (2010), Inferring episodic atmospheric iron fluxes in the Western South Atlantic, *Atmos. Environ.*, *44*(5), 703–712.

Falkowski, P. G. (1997), Evolution of the nitrogen cycle and its influence on the biological sequestration of CO2 in the ocean, *Nature*, *387*(6630), 272–275.

Fischer, A. C., J. J. Kroon, T. G. Verburg, T. Teunissen, and H. T. Wolterbeek (2007), On the relevance of iron adsorption to container materials in small-volume experiments on iron marine chemistry: Fe-55-aided assessment of capacity, affinity and kinetics, *Mar. Chem.*, *107*(4), 533–546.

Fok, A. K., Y. Lee, and R. D. Allen (1982), The Correlation of Digestive Vacuole Ph and Size with the Digestive Cycle in Paramecium-Caudatum, *J. Protozool.*, *29*(3), 409–414.

Forster, G., R. C. Upstill-Goddard, N. Gist, C. Robinson, G. Uher, and E. M. S. Woodward (2009), Nitrous oxide and methane in the Atlantic Ocean between 50°N and 52°S: Latitudinal distribution and sea-to-air flux, *Deep-Sea Res.Pt II*, *56*(15), 964–976.

Gaiero, D. M., F. Brunet, J. L. Probst, and P. J. Depetris (2007), A uniform isotopic and chemical signature of dust exported from Patagonia: Rock sources and occurrence in southern environments, *Chem. Geol.*, *238*(1–2), 107–120.

Gaiero, D. M., J.-L. Probst, P. J. Depetris, S. M. Bidart, and L. Leleyter (2003), Iron and other transition metals in Patagonian riverborne and windborne materials: Geochemical control and transport to the southern South Atlantic Ocean, *Geochim. Cosmochim. Acta*, *67*, 3603–3623.

Gerringa, L. J. A., M. J. W. Veldhuis, K. R. Timmermans, G. Sarthou, and H. J. W. de Baar (2006), Co-variance of dissolved Fe-binding ligands with phytoplankton characteristics in the Canary Basin, *Mar. Chem.*, *102*(3–4), 276–290.

Grasshoff, K., K. Kremling, and M. Ehrhardt (1999), Methods of Seawater analysis, Wiley-VCH Verlag, Weinheim (FRG).

Hassler, C. S., V. Schoemann, C. M. Nichols, E. C. V. Butler, and P. W. Boyd (2011), Saccharides enhance iron bioavailability to Southern Ocean phytoplankton, *Proc. Natl. Acad. Sci.*, *108*(3), 1076–1081.

Hayase, K., and N. Shinozuka (1995), Vertical distribution of fluorescent organic matter along with AOU and nutrients in the equatorial Central Pacific, *Mar. Chem.*, *48*(3–4), 283.

Heller, M. I., and P. L. Croot (2010a), Application of a Superoxide (O_2^-) thermal source (SOTS-1) for the determination and calibration of O_2^- fluxes in seawater, *Anal. Chim. Acta*, *667*, 1–13.

Heller, M. I., and P. L. Croot (2010b), Kinetics of superoxide reactions with dissolved organic matter in tropical Atlantic surface waters near Cape Verde (TENATSO), *J. Geophys. Res.*, *115*(C12), C12038.

Heller, M. I., and P. L. Croot (2010c), Superoxide Decay Kinetics in the Southern Ocean, *Environ. Sci. Technol.*, *44*(1), 191–196.

Heller, M. I., and P. L. Croot (2011), Superoxide decay as a probe for speciation changes during dust dissolution in Tropical Atlantic surface waters near Cape Verde, *Mar. Chem.*, *126*(1–4), 37–55.

Ito, Y., and A. Butler (2005), Structure of synechobactins, new siderophores of the marine cyanobacterium *Synechococcus* sp. PCC 7002, *Limnol. Oceanogr.*, *50*(6), 1918–1923.

Jickells, T. D., et al. (2005), Global Iron Connections Between Desert Dust, Ocean Biogeochemistry, and Climate, *Science*, *308*(5718), 67–71.

Johnson, M. S., N. Meskhidze, V. P. Kiliyanpilakkil, and S. Gassó (2011), Understanding the transport of Patagonian dust and its influence on marine biological activity in the South Atlantic Ocean, *Atmos. Chem. Phys.*, *11*(6), 2487–2502.

Jørgensen, L., C. A. Stedmon, T. Kragh, S. Markager, M. Middelboe, and M. Søndergaard (2011), Global trends in the fluorescence characteristics and distribution of marine dissolved organic matter, *Marine Chemistry*, *126*(1–4), 139–148.

Karl, D. M., M. J. Church, J. E. Dore, R. M. Letelier, and C. Mahaffey (2012), Predictable and efficient carbon sequestration in the North Pacific Ocean supported by symbiotic nitrogen fixation, *Proc. Natl. Acad. Sci.*, *109*(6), 1842–1849.

Karyampudi, V. M., et al. (1999), Validation of the Saharan dust plume conceptual model using lidar, Meteosat, and ECMWF data, *Bull. Am. Meteorol. Soc.*, *80*(6), 1045–1075.

Kitayama, S., et al. (2009), Controls on iron distributions in the deep water column of the North Pacific Ocean: Iron(III) hydroxide solubility and marine humic-type dissolved organic matter, *J. Geophys. Res.*, *114*.

Kitidis, V., A. P. Stubbins, G. Uher, R. C. Upstill Goddard, C. S. Law, and E. M. S. Woodward (2006), Variability of chromophoric organic matter in surface waters of the Atlantic Ocean, *Deep-Sea Res. Pt II*, *53*(14–16), 1666–1684.

Kuma, K., J. Nishioka, and K. Matsunaga (1996), Controls on iron(III) hydroxide solubility in seawater: The influence of pH and natural organic chelators, *Limnol. Oceanogr.*, *41*(3), 396–407.

Kuma, K., A. Katsumoto, H. Kawakami, F. Takatori, and K. Matsunaga (1998), Spatial variability of Fe(III) hydroxide solubility in the water column of the northern North Pacific Ocean, *Deep-Sea Res. Pt I*, *45*(1), 91–113.

Laglera, L. M., and C. M. G. van den Berg (2009), Evidence for geochemical control of iron by humic substances in seawater, *Limnol. Oceanogr.*, *54*(2), 610–619.

Laglera, L. M., G. Battaglia, and C. M. G. van den Berg (2007), Determination of humic substances in natural waters by cathodic stripping voltammetry of their complexes with iron, *Anal. Chim. Acta*, *599*(1), 58.

Lawaetz, A. J., and C. A. Stedmon (2009), Fluorescence Intensity Calibration Using the Raman Scatter Peak of Water, *Appl. Spectrosc.*, *63*(8), 936–940.

Li, Q. P., D. A. Hansell, and J. Z. Zhang (2008), Underway monitoring of nanomolar nitrate plus nitrite and phosphate in oligotrophic seawater, *Limnol. Oceanogr.-Meth. 6*, 319–326.

Liu, X. W., and F. J. Millero (1999), The solubility of iron hydroxide in sodium chloride solutions, *Geochim. Cosmochim. Acta*, *63*(19–20), 3487–3497.

Liu, X. W., and F. J. Millero (2002), The solubility of iron in seawater, *Mar. Chem.*, *77*(1), 43–54.

Ma, J., R. Del Vecchio, K. S. Golanoski, E. S. Boyle, and N. V. Blough (2010), Optical Properties of Humic Substances and CDOM: Effects of Borohydride Reduction, *Environ. Sci. Technol.*, *44*(14), 5395–5402.

Martinez, J. S., M. G. Haygood, and A. Butler (2001), Identification of a natural desferrioxamine siderophore produced by a marine bacterium, *Limnol. Oceanogr.*, *46*, 420–424.

Martinez, J. S., J. N. Carter-Franklin, E. L. Mann, J. D. Martin, M. G. Haygood, and A. Butler (2003), Bioinorganic Chemistry Special Feature: Structure and membrane affinity of a suite of amphiphilic siderophores produced by a marine bacterium, *PNAS*, *100*(7), 3754–3759.

Mawji, E., M. Gledhill, J. A. Milton, M. V. Zubkov, A. Thompson, G. A. Wolff, and E. P. Achterberg (2011), Production of siderophore type chelates in Atlantic Ocean waters enriched with different carbon and nitrogen sources, *Mar. Chem.*, *124*(1–4), 90–99.

Mawji, E., M. Gledhill, J. A. Milton, G. A. Tarran, S. Ussher, A. Thompson, G. A. Wolff, P. J. Worsfold, and E. P. Achterberg (2008), Hydroxamate Siderophores: Occurrence and Importance in the Atlantic Ocean, *Environ. Sci. Technol.*, *42*(23), 8675–8680.

McCormick, J. P., and T. Thomason (1978), Near-ultraviolet photooxidation of tryptophan. Proof of formation of superoxide ion, *J. Am. Chem. Soc.*, *100*(1), 312–313.

Mills, M. M., C. Ridame, M. Davey, J. La Roche, and R. J. Geider (2004), Iron and phosphorus co-limit nitrogen fixation in the eastern tropical North Atlantic, *Nature*, *429*(6989), 292–294.

Moore, C. M., et al. (2009), Large-scale distribution of Atlantic nitrogen fixation controlled by iron availability, *Nat. Geosci.*, *2*(12), 867–871.

Mopper, K., and C. A. Schultz (1993), Fluorescence as a possible tool for studying the nature and water column distribution of DOC components, *Mar. Chem.*, *41*(1–3), 229–238.

Murphy, J., and J. P. Riley (1962), A modified single solution method for the determination of phosphate in natural waters, *Anal. Chim. Acta*, *27*, 31–36.

Murphy, K. R., C. A. Stedmon, T. D. Waite, and G. M. Ruiz (2008), Distinguishing between terrestrial and autochthonous organic matter sources in marine environments using fluorescence spectroscopy, *Mar. Chem.*, *108*(1–2), 40–58.

Murphy, K. R., K. D. Butler, R. G. M. Spencer, C. A. Stedmon, J. R. Boehme, and G. R. Aiken (2010), Measurement of Dissolved Organic Matter Fluorescence in Aquatic Environments: An Interlaboratory Comparison, *Environ. Sci. Technol.*, *44*(24), 9405–9412.

Nakabayashi, S., M. Kusakabe, K. Kuma, and I. Kudo (2001), Vertical distributions of iron(III) hydroxide solubility and dissolved iron in the northwestern North Pacific Ocean, *Geophys. Res. Lett.*, *28*(24), 4611–4614.

Nakabayashi, S., K. Kuma, K. Sasaoka, S. Saitoh, M. Mochizuki, N. Shiga, and M. Kusakabe (2002), Variation in iron(III) solubility and iron concentration in the northwestern North Pacific Ocean, *Limnol. Oceanogr.*, *47*(3), 885–892.

Nakayama, Y., S. Fujita, K. Kuma, and K. Shimada (2011), Iron and humic-type fluorescent dissolved organic matter in the Chukchi Sea and Canada Basin of the western Arctic Ocean, *J. Geophys. Res.*, *116*(C7), C07031.

Nelson, N. B., D. A. Siegel, C. A. Carlson, and C. M. Swan (2010), Tracing global biogeochemical cycles and meridional overturning circulation using chromophoric dissolved organic matter, *Geophys. Res. Lett.*, *37*.

Nelson, N. B., D. A. Siegel, C. A. Carlson, C. Swan, W. M. Smethie, and S. Khatiwala (2007), Hydrography of chromophoric dissolved organic matter in the North Atlantic, *Deep-Sea Res. Pt. I*, *54*(5), 710–731.

Neogi, S. B., B. P. Koch, P. Schmitt-Kopplin, C. Pohl, G. Kattner, S. Yamasaki, and R. J. Lara (2011), Biogeochemical controls on the bacterial population in the eastern Atlantic Ocean, *Biogeosciences Discuss.*, *8*(4), 7791–7821.

Nishimura, S., K. Kuma, S. Ishikawa, A. Omata, and S.-i. Saitoh (2012), Iron, nutrients, and humic-type fluorescent dissolved organic matter in the northern Bering Sea shelf, Bering Strait, and Chukchi Sea, *J. Geophys. Res.*, *117*(C2), C02025.

O'Sullivan, D. W., P. J. Neale, R. B. Coffin, T. J. Boyd, and S. L. Osburn (2005), Photochemical production of hydrogen peroxide and methylhydroperoxide in coastal waters, *Mar. Chem.*, *97*(1–2), 14–33.

Omori, Y., T. Hama, M. Ishii, and S. Saito (2011), Vertical change in the composition of marine humic-like fluorescent dissolved organic matter in the subtropical western North Pacific and its relation to photoreactivity, *Mar. Chem.*, *124*(1–4), 38–47.

Poorvin, L., S. G. Sander, I. Velasquez, E. Ibisanmi, G. R. LeCleir, and S. W. Wilhelm (2011), A comparison of Fe bioavailability and binding of a catecholate siderophore with virus-mediated lysates from the marine bacterium Vibrio alginolyticus PWH3a, *J. Exp. Mar. Biol. Ecol.*, *399*(1), 43–47.

Powell, R. T., and J. R. Donat (2001), Organic complexation and speciation of iron in the South and Equatorial Atlantic, *Deep-Sea Res. Pt. II.*, *48*(13), 2877–2893.

Powell, R. T., and A. Wilson-Finelli (2003), Photochemical degradation of organic iron compelxing ligands in seawater, *Aquat. Sci.*, *65*, 367–374.

Quentel, F., C. Madec, and J. Courtot-coupez (1987), Determination of Humic Substances in Seawater by Electrochemistry (Mechanisms), *Anal. Lett.*, *20*(1), 47–62.

Rijkenberg, M. J. A., C. F. Powell, M. Dall'Osto, M. C. Nielsdottir, M. D. Patey, P. G. Hill, A. R. Baker, T. D. Jickells, R. M. Harrison, and E. P. Achterberg (2008), Changes in iron speciation following a Saharan dust event in the tropical North Atlantic Ocean, *Mar. Chem.*, *110*(1–2), 56–67.

Rue, E. L., and K. W. Bruland (1995), Complexation of Iron(III) by Natural Organic Ligands in the Central North Pacific as Determined by a New Competitive Ligand Equilibration/Adsorptive Cathodic Stripping Voltammetric Method, *Mar. Chem.*, *50*, 117–138.

Santana-Casiano, J. M., M. Gonzalez-Davila, and F. J. Millero (2006), The role of Fe(II) species on the oxidation of Fe(II) in natural waters in the presence of O_2 and H_2O_2, *Mar. Chem.*, *99*(1–4), 70–82.

Scapini, M. d., V. Conzonno, V. Balzaretti, and A. Cirelli (2010), Comparison of marine and river water humic substances in a Patagonian environment (Argentina), *Aquat. Sci.*, *72*(1), 1–12.

Schlosser, C., and P. L. Croot (2009), Controls on seawater Fe(III) solubility in the Mauritanian upwelling zone, *Geophys. Res. Lett.*, *36*, L18606, doi:18610.11029/12009GL038963.

Schlosser, C., C. L. De La Rocha, and P. L. Croot (2011), Effects of iron surface adsorption and sample handling on iron solubility measurements, *Mar. Chem.*, *127*(1–4), 48–55.

Schlosser, C., C. L. De La Rocha, P. Streu, and P. L. Croot (2012), Solubility of iron in the Southern Ocean, *Limnol. Oceanogr.*, *57*(3), 684–697.

Shaked, Y., A. B. Kustka, and F. M. M. Morel (2005), A general kinetic model for iron acquisition by eukaryotic phytoplankton, *Limnol. Oceanogr.*, *50*(3), 872–882.

Shimotori, K., K. Watanabe, and T. Hama (2012), Fluorescence characteristics of humic-like fluorescent dissolved organic matter produced by various taxa of marine bacteria, *Aquat. Microb. Ecol.*, *65*(3), 249–260.

Stedmon, C. A., and R. Bro (2008), Characterizing dissolved organic matter fluorescence with parallel factor analysis: a tutorial, *Limnol. Oceanogr.-Meth.*, *6*, 572–579.

Stedmon, C. A., S. Markager, and R. Bro (2003), Tracing dissolved organic matter in aquatic environments using a new approach to fluorescence spectroscopy, *Marine Chemistry*, *82*(3–4), 239–254.

Steigenberger, S., and P. L. Croot (2008), Identifying the processes controlling the Distribution of H_2O_2 in surface waters along a meridional transect in the Eastern Atlantic., *Geophys. Res. Lett.*, *35*, L03616, doi:03610.01029/02007GL032555.

Stramma, L., M. Visbeck, P. Brandt, T. Tanhua, and D. Wallace (2009), Deoxygenation in the oxygen minimum zone of the eastern tropical North Atlantic, *Geophys. Res. Lett.*, *36*.

Tagliabue, A., and C. Völker (2011), Towards accounting for dissolved iron speciation in global ocean models, *Biogeosciences Discuss.*, *8*, 2775–2810.

Takata, H., et al. (2004), Spatial variability of iron in the surface water of the northwestern North Pacific Ocean, *Mar. Chem.*, *86*, 139–157.

Tani, H., J. Nishioka, K. Kuma, H. Takata, Y. Yamashita, E. Tanoue, and T. Midorikawa (2003), Iron(III) hydroxide solubility and humic-type fluorescent organic matter in the deep water column of the Okhotsk Sea and the northwestern North Pacific Ocean, *Deep-Sea Res.*, *50*, 1063–1078.

Tarran, G. A., J. L. Heywood, and M. V. Zubkov (2006), Latitudinal changes in the standing stocks of nano- and picoeukaryotic phytoplankton in the Atlantic Ocean, *Deep-Sea Res. Pt. II*, *53*(14–16), 1516–1529.

Tyrrell, T., E. Maranon, A. J. Poulton, A. R. Bowie, D. S. Harbour, and E. M. S. Woodward (2003), Large-scale latitudinal distribution of Trichodesmium spp. in the Atlantic Ocean, *J. Plankton Res.*, *25*(4), 405–416.

Veldhuis, M. J. W., G. W. Kraay, and K. R. Timmermans (2001), Cell death in phytoplankton: correlation between changes in membrane permeability, photosynthetic activity, pigmentation and growth, *Eur. J. Phycol.*, *36*(2), 167–177.

Wagener, T., E. Pulido-Villena, and C. Guieu (2008), Dust iron dissolution in seawater: Results from a one-year time-series in the Mediterranean Sea, *Geophys. Res. Lett.*, *35*(16).

Yamashita, Y., and E. Tanoue (2003a), Distribution and alteration of amino acids in bulk DOM along a transect from bay to oceanic waters, *Mar. Chem.*, *82*(3–4), 145–160.

Yamashita, Y., and E. Tanoue (2003b), Chemical characterization of protein-like fluorophores in DOM in relation to aromatic amino acids, *Mar. Chem.*, *82*(3–4), 255–271.

Yamashita, Y., and E. Tanoue (2008), Production of bio-refractory fluorescent dissolved organic matter in the ocean interior, *Nat. Geosci.*, *1*(9), 579–582.

Yamashita, Y., and E. Tanoue (2009), Basin scale distribution of chromophoric dissolved organic matter in the Pacific Ocean, *Limnol. Oceanogr.*, *54*(2), 598–609.

Yamashita, Y., A. Tsukasaki, T. Nishida, and E. Tanoue (2007), Vertical and horizontal distribution of fluorescent dissolved organic matter in the Southern Ocean, *Mar. Chem.*, *106*(3–4), 498–509.

Yuan, J., and A. M. Shiller (1999), Determination of Subnanomolar Levels of Hydrogen Peroxide in Seawater by Reagent-Injection Chemiluminescence Detection, *Anal. Chem.*, *71*, 1975–1980.

Yuan, J., and A. M. Shiller (2001), The distribution of hydrogen peroxide in the southern and central Atlantic ocean, *Deep-Sea Res. Pt. II*, *48*, 2947–2970.

Zafiriou, O. C., J. Joussot-Dubien, R. G. Zepp, and R. G. Zika (1984), Photochemistry of natural waters, *Environ. Sci. Technol.*, *18*(12), 358A–371A.

Zubkov, M. V., G. A. Tarran, I. Mary, and B. M. Fuchs (2008), Differential microbial uptake of dissolved amino acids and amino sugars in surface waters of the Atlantic Ocean, *J. Plankton Res.*, *30*(2), 211–220.

Author Query Form

Journal: Global Biogeochemical Cycles

Article: gbc_20004

Dear Author,

During the copyediting of your paper, the following queries arose. Please respond to these by annotating your proofs with the necessary changes/additions.

- If you intend to annotate your proof electronically, please refer to the E-annotation guidelines.
- If you intend to annotate your proof by means of hard-copy mark-up, please refer to the proof mark-up symbols guidelines. If manually writing corrections on your proof and returning it by fax, do not write too close to the edge of the paper. Please remember that illegible mark-ups may delay publication.

Whether you opt for hard-copy or electronic annotation of your proofs, we recommend that you provide additional clarification of answers to queries by entering your answers on the query sheet, in addition to the text mark-up.

Query No.	Query	Remark
Q1	AUTHOR: Please spell out CT.	
Q2	AUTHOR: Please clarify 'P.S. Polarstern' Is this different from 'R/V Polarstern'?	
Q3	AUTHOR: Please provide title of paper and year of submission.	
Q4	"Wedborg et al., 2007" is cited in text but not given in the reference list. Please provide details in the list or delete the citation from the text.	
Q5	"Dubnick et al., 2010" is cited in text but not given in the reference list. Please provide details in the list or delete the citation from the text.	
Q6	"Chanudet et al., 1987" is cited in text but not given in the reference list. Please provide details in the list or delete the citation from the text.	
Q7	If reference Chen et al., 2004 has now been published online, please add relevant year/DOI information. If this reference has now been published in print, please add relevant page information.	
Q8	Please provide the city location of publisher for Reference Cooper et al., 1988.	
Q9	If reference Croot et al., 2011 has now been published online, please add relevant year/DOI information. If this reference has now been published in print, please add relevant volume and page information.	
Q10	If reference Kitayama et al., 2009 has now been published online, please add relevant year/DOI information. If this reference has now been published in print, please add relevant page information.	
Q11	If reference Nelson et al., 2010 has now been published online, please add relevant year/DOI information. If this reference has now been published in print, please add relevant page information.	
Q12	If reference Stramma et al., 2009 has now been published online, please add relevant year/DOI information. If this reference has now been published in print, please add relevant page information.	

Query No.	Query	Remark
Q13	If reference Wagener et al., 2008 has now been published online, please add relevant year/DOI information. If this reference has now been published in print, please add relevant page information.	

USING e-ANNOTATION TOOLS FOR ELECTRONIC PROOF CORRECTION

Required software to e-Annotate PDFs: Adobe Acrobat Professional or Adobe Reader (version 8.0 or above). (Note that this document uses screenshots from Adobe Reader X)
The latest version of Acrobat Reader can be downloaded for free at: http://get.adobe.com/reader/

Once you have Acrobat Reader open on your computer, click on the Comment tab at the right of the toolbar:

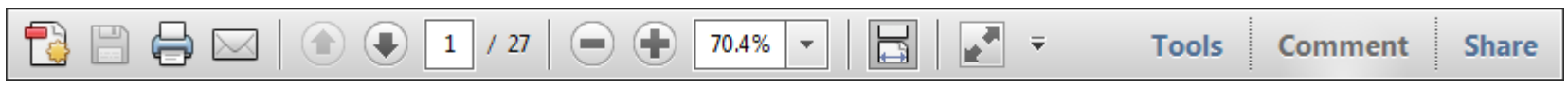

This will open up a panel down the right side of the document. The majority of tools you will use for annotating your proof will be in the Annotations section, pictured opposite. We've picked out some of these tools below:

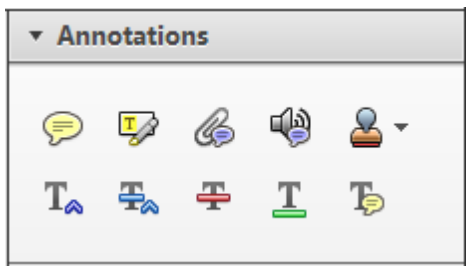

1. Replace (Ins) Tool – for replacing text.

Strikes a line through text and opens up a text box where replacement text can be entered.

How to use it

- Highlight a word or sentence.
- Click on the Replace (Ins) icon in the Annotations section.
- Type the replacement text into the blue box that appears.

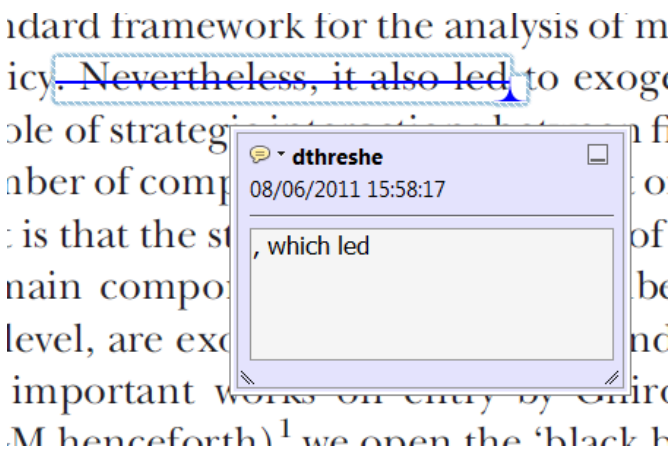

2. Strikethrough (Del) Tool – for deleting text.

Strikes a red line through text that is to be deleted.

How to use it

- Highlight a word or sentence.
- Click on the Strikethrough (Del) icon in the Annotations section.

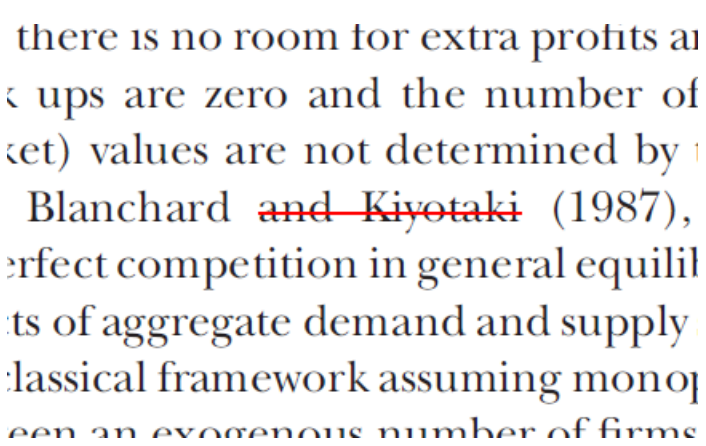

3. Add note to text Tool – for highlighting a section to be changed to bold or italic.

Highlights text in yellow and opens up a text box where comments can be entered.

How to use it

- Highlight the relevant section of text.
- Click on the Add note to text icon in the Annotations section.
- Type instruction on what should be changed regarding the text into the yellow box that appears.

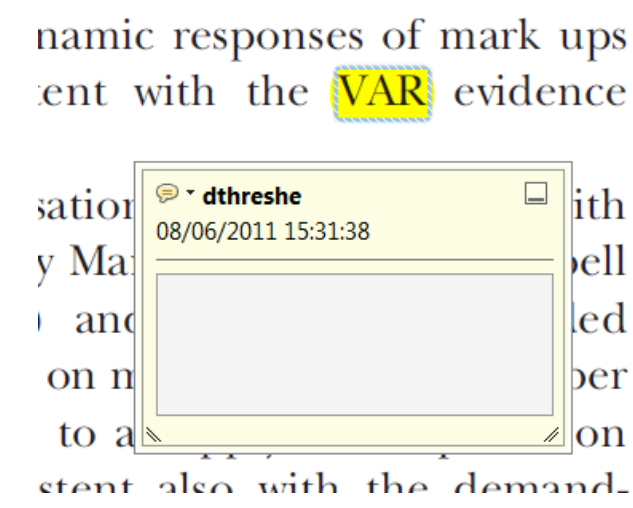

4. Add sticky note Tool – for making notes at specific points in the text.

Marks a point in the proof where a comment needs to be highlighted.

How to use it

- Click on the Add sticky note icon in the Annotations section.
- Click at the point in the proof where the comment should be inserted.
- Type the comment into the yellow box that appears.

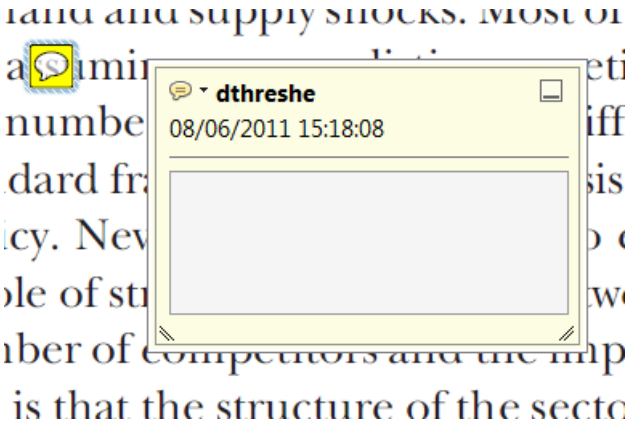

USING e-ANNOTATION TOOLS FOR ELECTRONIC PROOF CORRECTION

5. Attach File Tool – for inserting large amounts of text or replacement figures.

Inserts an icon linking to the attached file in the appropriate pace in the text.

How to use it

- Click on the Attach File icon in the Annotations section.
- Click on the proof to where you'd like the attached file to be linked.
- Select the file to be attached from your computer or network.
- Select the colour and type of icon that will appear in the proof. Click OK.

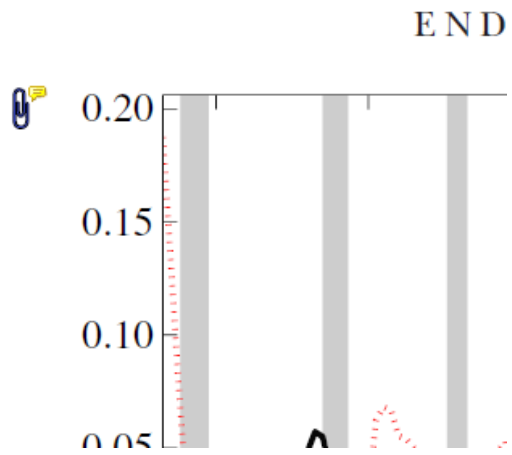

6. Add stamp Tool – for approving a proof if no corrections are required.

Inserts a selected stamp onto an appropriate place in the proof.

How to use it

- Click on the Add stamp icon in the Annotations section.
- Select the stamp you want to use. (The Approved stamp is usually available directly in the menu that appears).
- Click on the proof where you'd like the stamp to appear. (Where a proof is to be approved as it is, this would normally be on the first page).

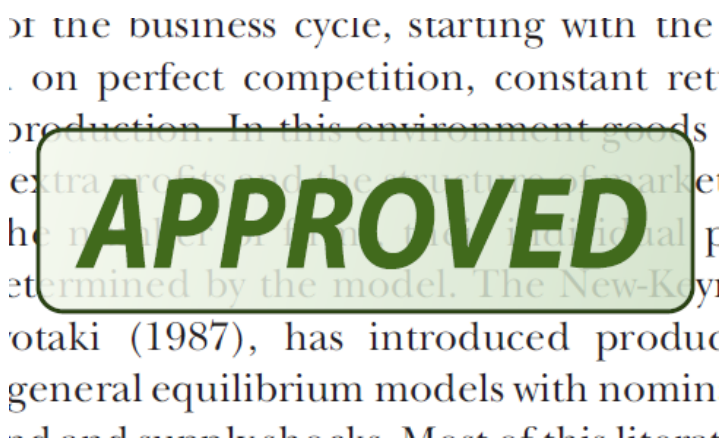

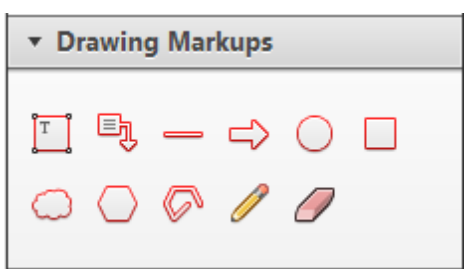

7. Drawing Markups Tools – for drawing shapes, lines and freeform annotations on proofs and commenting on these marks.

Allows shapes, lines and freeform annotations to be drawn on proofs and for comment to be made on these marks..

How to use it

- Click on one of the shapes in the Drawing Markups section.
- Click on the proof at the relevant point and draw the selected shape with the cursor.
- To add a comment to the drawn shape, move the cursor over the shape until an arrowhead appears.
- Double click on the shape and type any text in the red box that appears.

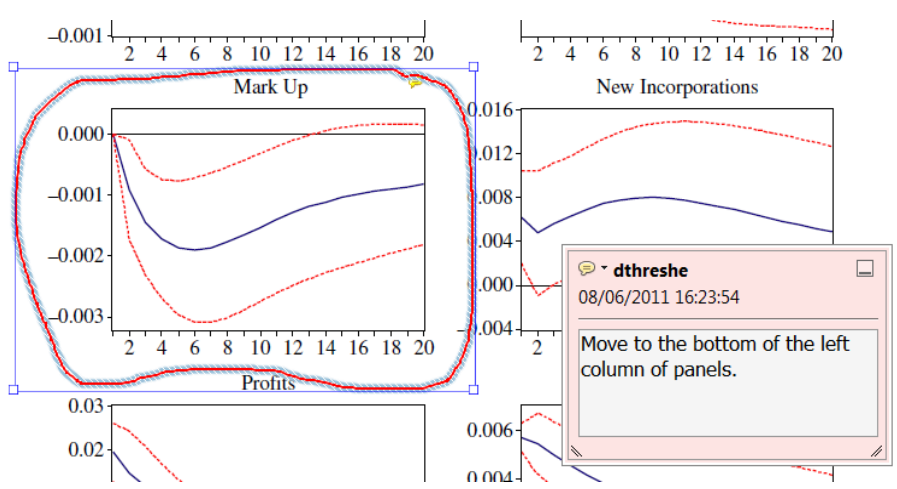

For further information on how to annotate proofs, click on the Help menu to reveal a list of further options:

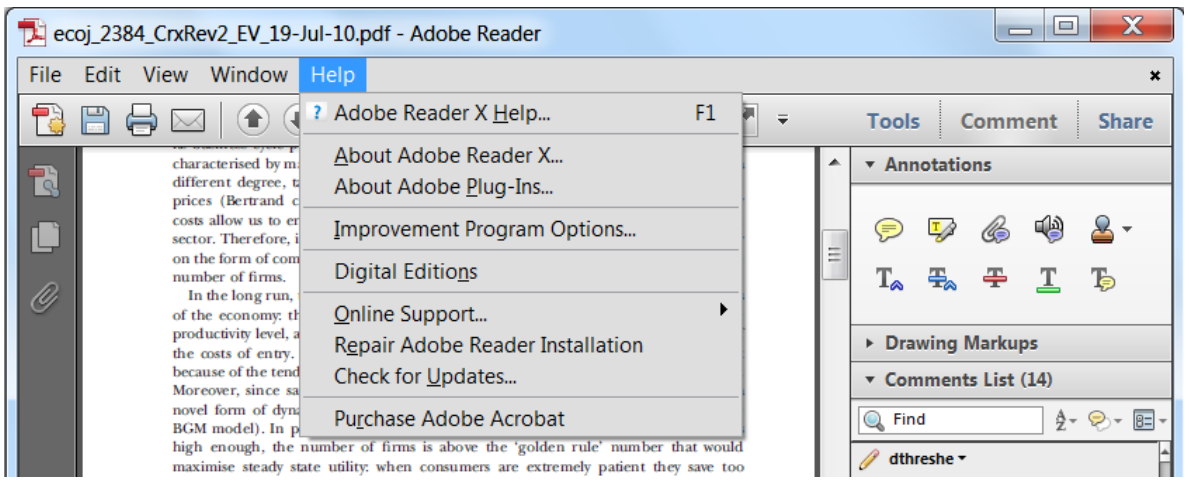

AGU American Geophysical Union

WILEY

Article Page Charge Form

Instructions:

1. Enter the Article Number as it appears on your article.
2. Enter the final number of Pages in Article as it appears in your proof.
3. Select the Journal Name from the dropdown list; this will determine the Publication Fee and the Excess Length Fee (if applicable).
4. Check and confirm your selections, as they will generate your Total Cost.
    a. Publication Fee refers to the flat fee for article publication per journal.
    b. Excess Length Fee ($250 per page) applies to pages >13 for all journals, except *Geophysical Research Letters*, for which it applies to pages >5.
5. Check the box for OnlineOpen (which will negate your page fees) if you'd like for your article to be open access and fill out the form on this page: https://authorservices.wiley.com/bauthor/onlineopen_order.asp.
6. Authorize Wiley to process a final invoice upon publication in an issue via the Signature line.
7. Enter the billing name and address. The Wiley Reprints Department will use the information provided to invoice charges.
8. Click "Submit" to e-mail this form as an attachment to the Production Editor. If your local mail client does not launch, please save this form and send it as an attachment to _____.

Article Number	
Pages in Article	
Journal Name	
(select a journal)	
Publication Fee	$ 0
Excess Length Fee per Page	$ 0
OnlineOpen?	☐
Total Cost: $ 0	

Signature: _____

Fill in all billing contact information below to accept the **Total Cost** on the left.

Name:

Address:

Phone:

E-mail:

SUBMIT